General Disclaimer

One or more of the Following Statements may affect this Document

- This document has been reproduced from the best copy furnished by the organizational source. It is being released in the interest of making available as much information as possible.

- This document may contain data, which exceeds the sheet parameters. It was furnished in this condition by the organizational source and is the best copy available.

- This document may contain tone-on-tone or color graphs, charts and/or pictures, which have been reproduced in black and white.

- This document is paginated as submitted by the original source.

- Portions of this document are not fully legible due to the historical nature of some of the material. However, it is the best reproduction available from the original submission.

NASA CR-144482
ERIM 102100-21-F
E7.6-10186

Final Report

SKYLAB REMOTE BATHYMETRY EXPERIMENT

DAVID R. LYZENGA and FABIAN C. POLCYN, Principal Investigator
Infrared and Optics Division

JANUARY 1976

Prepared for

NATIONAL AERONAUTICS AND SPACE ADMINISTRATION

Lyndon B. Johnson Space Center
Houston, Texas 77058
Contract No. NAS9-13278
Technical Monitor: Mr. Z. Burns/TF6

ENVIRONMENTAL
RESEARCH INSTITUTE OF MICHIGAN
FORMERLY WILLOW RUN LABORATORIES, THE UNIVERSITY OF MICHIGAN
BOX 618 • ANN ARBOR • MICHIGAN 48107

TECHNICAL REPORT STANDARD TITLE PAGE

1. Report No.	2. Government Accession No.	3. Recipient's Catalog No.
NASA CR-ERIM 102100-21-F		

4. Title and Subtitle	5. Report Date
SKYLAB REMOTE BATHYMETRY EXPERIMENT	JANUARY 1976
	6. Performing Organization Code

7. Author(s)	8. Performing Organization Report No.
David R. Lyzenga and Fabian C. Polcyn P.I.	102100-21-F

9. Performing Organization Name and Address	10. Work Unit No.
Environmental Research Institute of Michigan Infrared and Optics Division P. O. Box 618 Ann Arbor, Michigan 48107 (313) 994-1200	11. Contract or Grant No. NAS9-13278
	13. Type of Report and Period Covered Final Report
12. Sponsoring Agency Name and Address National Aeronautics and Space Administration Johnson Space Center Houston, Texas 77058	14. Sponsoring Agency Code

15. Supplementary Notes

Mr. Zack Byrns (Code TF6) monitored this work.

16. Abstract

Test sites of different water quality and bottom topography have been used to test for maximum water depth penetration using the Skylab S-192 MSS for measurement of nearshore coastal bathymetry. Sites under investigation lie along the Lake Michigan coastline where littoral transport acts to erode sand bluffs and endangers developments along 1,200 miles of shore, and off the coast of Puerto Rico where unreliable shoal location and depth information constitutes a safety hazard to navigation.

Recent collisions of oil carrying supertankers with shallow obstructions highlight the need for an up-dating of world navigation charts especially in well traveled zones.

The S-192 and S-190A and B provide data on underwater features because of water transparency in the blue/green portion of the spectrum. Depth to 20 meters has been measured with the S-192 in the Puerto Rico test site. The S-190B photography with its improved spatial resolution clearly delineates the triple sand bar topography in the Lake Michigan test site.

Several processing techniques have been employed to test for maximum depth measurement with least error. The results are useful for helping to determine an optimum spectral bandwidth for future space sensors that will increase depth measurements for different water attenuation conditions where a bottom reflection is detectable.

17. Key Words	18. Distribution Statement
Remote sensing Bathymetry Shoal detection Skylab Water depth	Initial distribution is listed at the end of this document.

19. Security Classif. (of this report)	20. Security Classif. (of this page)	21. No. of Pages	22. Price
Unclassified	Unclassified	64	

PREFACE

The general objective of this project was to determine the improvement in the measurement of water depth from space using the Skylab Earth Resources Experiment Package notably the S-192 multispectral scanner and the S-190B camera system. This work continues a research program at ERIM conducted since 1969 as to the feasibility of remote bathymetry from aircraft or spacecraft altitude while relying on signal processing of reflected sunlight obtained in narrow spectral bands in the blue-green portion of spectrum. Previous research with multispectral scanners mounted in aircraft was sponsored by the National Oceanic and Atmospheric Agency's Spacecraft Oceanography Group (formerly of the Naval Oceanographic Office) under the direction of John Sherman III. Subsequently, LANDSAT 1 data was used to test the concept from spacecraft altitudes under Contract NAS5-21783, Task I.

This report is submitted in fulfillment of NASA Contract NAS9-13278. The Principal Investigator for the project was Fabian C. Polcyn and the work was carried out by the Infrared and Optics Division of ERIM under the direction of Mr. Richard R. Legault.

CONTENTS

1. INTRODUCTION 7

2. METHODS OF EXTRACTION OF DEPTH INFORMATION 10

3. DISCUSSION OF RESULTS 15
3.1 Pass 6: Southwestern Puerto Rico 15
3.1.1 Southern Coast 15
3.1.2 Western Coast 23
3.2 Pass 14: Central Lake Michigan Shoreline 31
3.3 Pass 54: Eastern Puerto Rico 41
3.3.1 Escollo de Arenas 41
3.3.2 Aves (Bird) Island 46

4. CONCLUSIONS 52

5. RECOMMENDATIONS 54

APPENDIX: ERROR ANALYSIS 56

REFERENCES 63

DISTRIBUTION LIST 64

FIGURES

1. S-190B Photograph of Southwestern Puerto Rico, (Pass 6 - June 9, 1973) 16

2. Processed S-192 Imagery for Southwestern Puerto Rico (Pass 6 - June 9, 1973).
   (a) Band 3: 0.50-0.55 μm 17
   (b) Band 11: 1.55-1.73 μm 18
   (c) Band 13: 10.2-12.5 μm 19

3. Bathymetric Chart for Southern Coast of Puerto Rico, Made from S-192 Band 3. 21

4. Portion of Coast and Geodetic Survey Chart 901, Showing Southern Coast of Puerto Rico 22

5. S-192 Band 2 and 3 Signals Versus Depth, Escollo Negro Area (Pass 6 - June 9, 1973). 25

6. Bathymetric Chart for Western Coast of Puerto Rico, Made from S-192 Bands 2 and 3. 26

7. Portion of Coast and Geodetic Survey Chart 901, Showing Western Coast of Puerto Rico. 27

8. Calculated and Chart Depths Along Line 1450 (Escollo Negro). 28

9. Calculated and Chart Depths Along Line 1440 (Escollo Negro). 29

10. S-190B Photograph of Eastern Lake Michigan, (Pass 14 - August 5, 1973). 32

11. Processed S-192 Imagery for Eastern Lake Michigan (Pass 14 - August 5, 1973.)
   (a) Band 3: 0.50-0.55 μm 33
   (b) Band 13: 10.2-12.5 μm 34

12. Enlargement of S-190B Photograph Showing Multiple Sand Bar Structure Along the Michigan Coastline. 35

13. S-192 Band 3 and 4 Data Values Versus Line Number for Transect Perpendicular to Shoreline 1 Mile South of Pentwater, Michigan. 37

14. S-190 Film Density Versus Distance from Shoreline for the Same Transect as in Figure 13. 38

15. Portion of Lake Survey Chart 77, Showing Lake Michigan Shoreline Near Pentwater, Michigan. 40

16. S-190B Photograph of Eastern Puerto Rico, (Pass 54 - November 30, 1973). 42

17. Processed S-192 Imagery for Eastern Puerto Rico, (Pass 54- November 30, 1973). Band 2 (.45 - .50 μm). 43

18. Portion of Coast and Geodetic Survey Chart 904, Showing Escollo de Arenas. 44

19. Comparison of Water Depth (Top Curve), S-192 Data Values (Center Curve), and S-190B Film Density (Lower Curve) for Transect Through the Escollo de Arenas (Pass 54- November 30, 1973). 45

20. Enlargement of S-190B Photograph Showing Aves (Bird) Island (Pass 54 - November 30, 1973). 48

21 Portion of Naval Oceanographic Chart 2551, Showing Aves (Bird) Island. 49

22. Densitometer Trace of S-190B Photograph for Transect Through Aves Island Shown in Figure 21.. 50

23. Comparison of Total Error for Three Depth Algorithms 62

SKYLAB REMOTE BATHYMETRY EXPERIMENT

1

INTRODUCTION

The research reported here is an outgrowth and continuation of previous research projects carried out at the Environmental Research Institute of Michigan for the purpose of developing methods of extracting water-depth information from multispectral scanner data collected by aircraft and satellites [1-4]. In particular, reference [4] describes three such methods which were successfully applied to ERTS-1 data from the Caribbean and Lake Michigan. The present report describes the application of these methods to data collected by the Earth Resources Experiment Package (EREP) of the Skylab program. In addition, this report contains an examination of the accuracy of the results as compared with published navigational charts, and an analysis of the types and magnitudes of errors inherent in each computational method.

The application potential of this technique can be seen from the recent announcements of losses of valuable crude oil as a result of collision of supertankers in different shipping lanes around the world. In general, world navigation charts are not current due to length of time for ship collection of data and subsequent map making and the dynamic processes for shifting sand bars and creating new shoals after storms. Also charts contain notations of shoal areas that are not verified in their depth or their location is known only approximately. Space acquired data offers the potential for providing more up-to-date information for navigation purposes thereby helping to reduce losses to life and property.

The data used in this research included the S-192 (multispectral scanner) and S-190 (photographic) products from all three Skylab missions. The locations and dates of the three principal data sets were:

Skylab 2, Pass 6: Southwestern Puerto Rico - June 9, 1973
Skylab 3, Pass 14: Central Lake Michigan - August 5, 1973
Skylab 4, Pass 54: Eastern Puerto Rico - November 30, 1973

Photographic products from several other passes were received, but were considered to be too cloudy to be useful for analysis. Data were received in the form of photographic transparencies (S-190 A and B), magnetic tapes containing the S-192 scanner data, and screening films made from these tapes. Processing of the films included enlarging and printing by ERIM's photographic laboratory, and in some cases scanning portions of the films with a Jarrell-Ash densitometer. Magnetic tapes were first converted to ERIM format on the University of Michigan's IBM 370 computer, and subsequently processed on ERIM's IBM 7094 computer.

The end-product of the digital processing is a computer-generated map on which different symbols are printed corresponding to various ranges of water depth. In this report two such maps are presented for portions of the southern and western coasts of Puerto Rico. On both maps, depths from 0 to 15 meters are indicated in 3 meter intervals by means of five symbols. A sixth symbol indicates a depth from 15 to 20 meters, and a seventh indicates a depth greater than 20 meters. In the case of the Lake Michigan data set, the number of points at which the depth could be computed was too small to justify or require such a display, and the results are presented in graphical form along a transect perpendicular to the shoreline. The same is true of the Eastern Puerto Rico data set, where a single transect through the Escollo de Arenas is presented as a means of comparing the S-190B film density with the S-192 data values and the water depth.

This report is organized chronologically, in the order in which the data were collected, received, and processed. The steps taken in analyzing the data are described and the results are presented and

discussed for each test site. Conclusions are stated in the last section, and an error analysis is included in the Appendix.

2

METHODS OF EXTRACTION OF DEPTH INFORMATION

The Skylab multispectral scanner (S-192) receives energy in 13 spectral bands. The scanner operates in a linear mode, so the signal recorded in each band is proportional to the radiance received in the corresponding wavelength interval. That is,

$$V_i = k_i R_i \tag{1}$$

where R_i is the radiance in band i at the detector and k_i is the sensitivity constant for the detector.

The radiance observed over shallow water is the result of sunlight reflecting from the bottom and the water surface, as well as of the scattering of sunlight in the water and the atmosphere. That part of the signal resulting from bottom reflection contains information about the depth of the water through which the light has passed. In order to extract this information, one must first separate the bottom-reflection signal from the rest of the observed signal, and then determine how this signal is related to the water depth.

Assuming the linear relationship (see Eq. 1) is correct, the signal observed over shallow water may be expressed as follows:

$$V_i = k_i R_{pi} + k_i \tau_i R_{si} + k_i \tau_i \frac{H_i}{\pi} \rho_i \frac{1}{n^2} e^{-\alpha_i (\sec\theta + \sec\phi) z} \tag{2}$$

where R_{pi} = atmospheric path radiance
τ_i = atmospheric transmittance
R_{si} = radiance resulting from (water) surface reflection
H_i = solar irradiance incident on water surface
ρ_i = bottom reflectance
n = index of refraction of water
α_i = attenuation coefficient of water
θ = angle of observation (under water)
ϕ = solar-zenith angle (under water)
z = water depth

This equation neglects volume scattering of sunlight from the water itself, which is usually small compared to the other components when conditions are favorable (i.e., when the water is fairly clear).

The first term of this equation accounts for the scattering of sunlight by the atmosphere; the second for the specular reflection of diffuse sky radiation by the water surface. The reflection of direct sunlight from the water surface into the scanner, known as sun glint, is avoided by restricting angles of observation to less than the solar-zenith angle.

Since these two terms contain no information about the water depth, they are considered as the background signal which must be removed before the actual depth processing is done. This background signal,

$$V_{bi} = k_i R_{pi} + k_i \tau_i R_{si} \qquad (3)$$

may be determined by scanning over deep water, where there is no bottom-reflected signal. When this background signal is subtracted from the data, the remainder represents the light which has been

reflected from the bottom and attenuated in the intervening water layer. From Equation (2), this part of the signal may be expressed as

$$\Delta V_i = V_i - V_{bi} = k_i \tau_i \frac{H_i}{\pi} \rho_i \frac{1}{n^2} e^{-\alpha_i (\sec \theta + \sec \phi) z} \qquad (4)$$

The depth dependence of this signal arises from the attenuation of light in the water, expressed by the exponential factor in this equation.

Three methods of extracting water depth from the multispectral data have been used in the research reported, the single channel method, the ratio method, and the optimum-decision-boundary method. The single channel method works best when uniform conditions prevails in bottom reflectivity and water absorption characteristics. The ratio method yields the smallest error due to changes in the bottom reflectivity or water quality, but is susceptible to errors due to noise or changes in the surface-reflected signals. By using two channels, quantitative measurement of depth is obtained at the expense of calculating depths to the maximum depth of the second channel which is less than the maximum depth from the best penetrating channel.

The optimum-decision-boundary technique is not limited in this way and gives the best results when two equally penetrating channels are used. The best method for any given application area depends on the data quality, channels available, and type of changes occurring in the scene.

For the single channel method, the depth z is

$$Z = - \frac{1}{\alpha f} \ln \frac{L_b}{L_o} \qquad (5)$$

where L_o = radiance at zero water depth
α = water attenuation coefficient
f = sec θ + sec ϕ
θ = scan angle (under water)
ϕ = solar zenith angle (under water)
L_b = bottom reflected signal

Calculation of errors with this method (see Appendix) shows that the error due to bottom changes is independent of depth, the error due to water attenuation changes in proportion to depth, and the error due to noise or surface fluctuations increases exponentially with depth. Therefore, at large depths, the latter type of error is always predominant.

In the ratio method, the radiance is measured in two channels i and j and the water depth is calculated using the following equation:

$$z = \frac{1}{(\alpha_j - \alpha_i) f} \ln\left(\frac{L_{b_i}}{L_{o_i}} \frac{L_{o_j}}{L_{b_j}}\right) \tag{6}$$

where symbols are defined as before but for different spectral channels.

The advantage of this method is that in some cases, a pair of channels can be found in which the ratio of the bottom reflectivities remains constant throughout the scene, or that the changes due to absorption differences are nearly the same for all wavelengths.

In the optimum-decision-boundary method the depth is calculated by the following expression

$$z = \frac{1}{(\alpha_i^2 + \alpha_j^2) f} \left[\alpha_i \ln \frac{L_{b_i}}{L_{o_i}} + \alpha_j \ln \frac{L_{b_j}}{L_{o_j}}\right] \tag{7}$$

In some cases by choosing spectral channels where reflectivities are negatively correlated, the error due to changes in bottom reflectivity may be reduced.

In this method, the error due to noise or surface reflectance changes is smallest if the two attenuation coefficients are equal or nearly equal.

A total error comparison was conducted for the three methods used and the results are given in the Appendix.

3
DISCUSSION OF RESULTS

3.1 PASS 6: SOUTHWESTERN PUERTO RICO

3.1.1 SOUTHERN COAST

On June 9, 1973 at 15:16:30 GMT, Skylab-2 passed over the southwest corner of Puerto Rico at a ground heading of 137.5° (approximately southeast) at an altitude of 440 km. The solar zenith angle at this time was 17.5°. Most of the southern coast was under clear skies, but a large bank of clouds covered the center of the island and extended over parts of the west coast. Photographic products and screening films were received at ERIM in late 1973, and a test tape containing six channels of data over the southern coast only was received early in 1974.

Upon receipt of the magnetic tape, the data was read and copied onto a new tape in a format compatible with the programs developed at ERIM for processing multispectral scanner data. An initial digital map was then made in order to locate line and point numbers of recognizable features on the map. Some analysis was also made of data quality, and band 3 (.50–.55 μm) was identified as the most useful channel from the point of view of water penetration and noise.

Some of the photographic and scanner imagery in this site are shown in Figures 1 and 2. Figure 2a shows good water penetration while 2b in the near infrared region shows only land/cloud and surface water boundary. Figure 2c gives the thermal image for the same area. No correlations were seen in this image between off-shore currents and shallow coastal zones either because no temperature gradients existing or the difference in temperature sensitivity of S-192 was too large for subtle differences to be detected. Color coding to improve contrast also did not show any detectable gradients.

Working on the assumption that the bottom reflectivity and water quality were fairly uniform throughout the scene, (also

FIGURE 1. S-190B PHOTOGRAPH OF SOUTHWESTERN PUERTO RICO
(PASS 6 - JUNE 9, 1973)

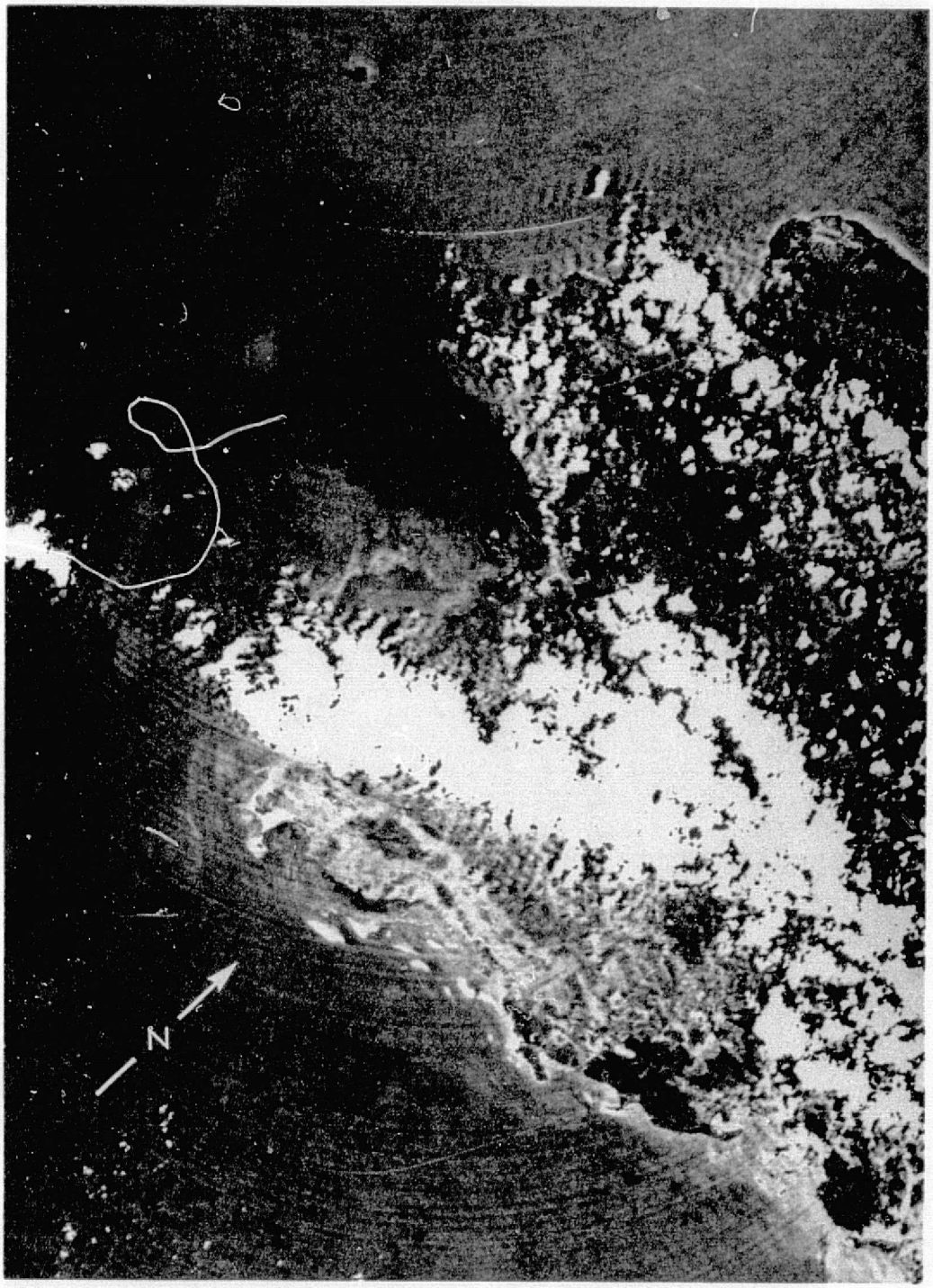

FIGURE 2a. PROCESSED S-192 IMAGERY FOR SOUTHWESTERN PUERTO RICO (PASS 6 - JUNE 9, 1973) BAND 3: 0.50-0.55 μm

FIGURE 2b. PROCESSED S-192 IMAGERY FOR SOUTHWESTERN PUERTO RICO (PASS 6 - JUNE 9, 1973) BAND 11: 1.55-1.73 μm

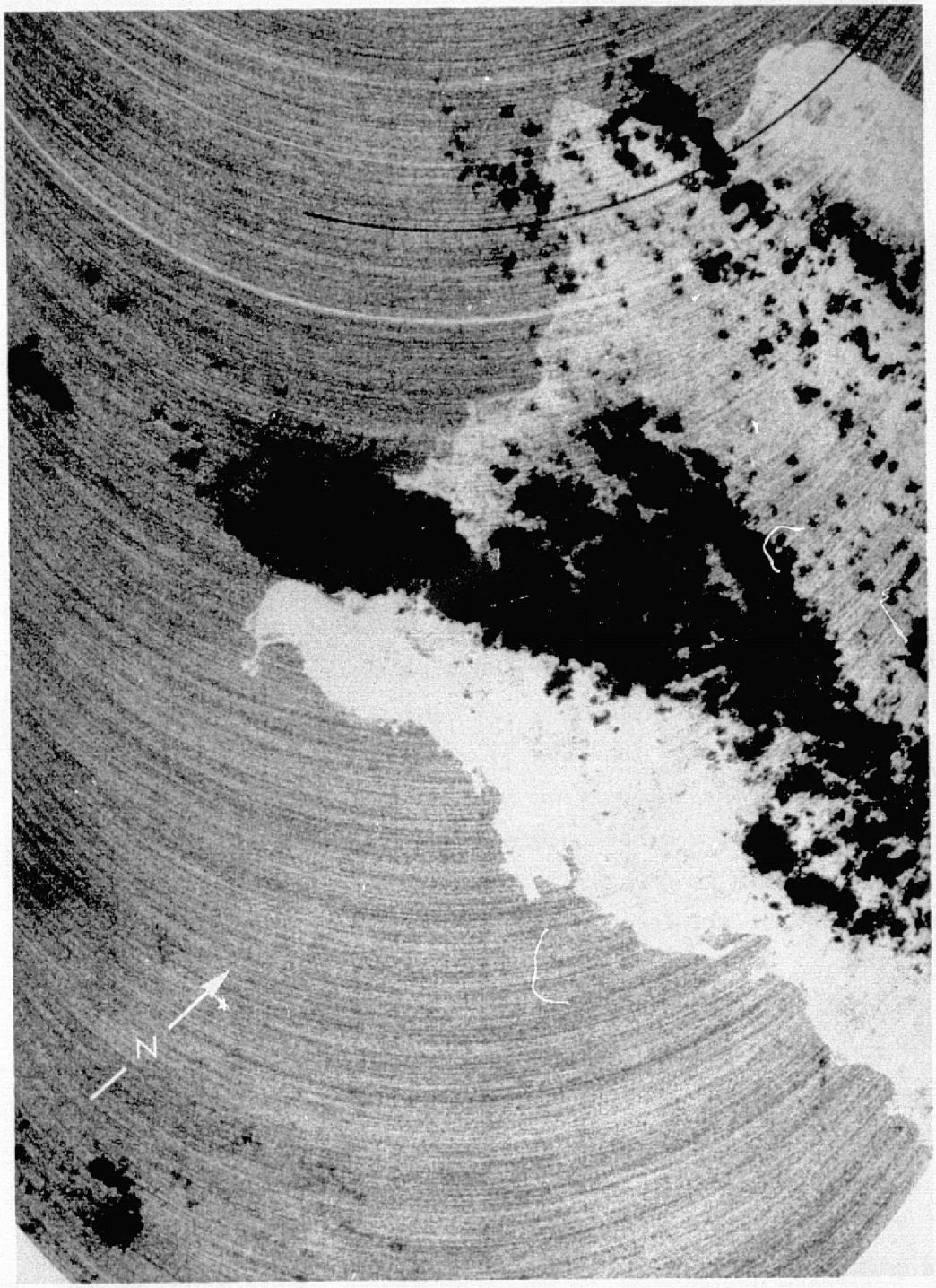

FIGURE 2c. PROCESSED S-192 IMAGERY FOR SOUTHWESTERN PUERTO RICO (PASS 6 - JUNE 9, 1973) BAND 13: 10.2-12.5 μm

confirmed by inspection of S-190B photography) an attempt was then made to associate data values in the visible band 5 with depths indicated on Coast and Geodetic Survey Chart 901. (A tide table was also consulted, and it was found that tidal variations were on the order of one foot in this area and could thus be neglected.) The digital signal observed over deep water was found to be approximately 68 counts. Subtracting this value from the shallow-water signals and plotting them versus depth on semi-log paper, the attenuation coefficient of the water was found to be about $.08m^{-1}$. This value corresponds with published values [1] for mean oceanic water.

The relationship thus established between data values and water depth was used to generate a water depth map (Figure 3) for the southern coast of Puerto Rico from Cabo Rojo to Punta Montalva. Figure 4 shows a corresponding portion of Coast and Geodetic Survey Chart 901.

Several features of this depth map deserve comment. First, the curved streaks running through the data are caused by low-frequency noise. In an attempt to reduce this noise, the data was smoothed 2 lines x 2 points, so that each pixel in Figure 3 actually represents the average of four original pixels. However, a significant amount of low-frequency noise remains, and cannot be removed without further degradation of spatial resolution.

Second, although there appears to be fairly good general agreement between the digital depth map and the Coast and Geodetic Survey Chart, there are a number of anomalous areas where the water depth is overestimated, notably to the east of Cabo Rojo and Arrecife Margarita. It was at first assumed that these were due to the presence of dark bottom materials, and an attempt was made to remove the anomalies using the ratio method described in the Appendix. This

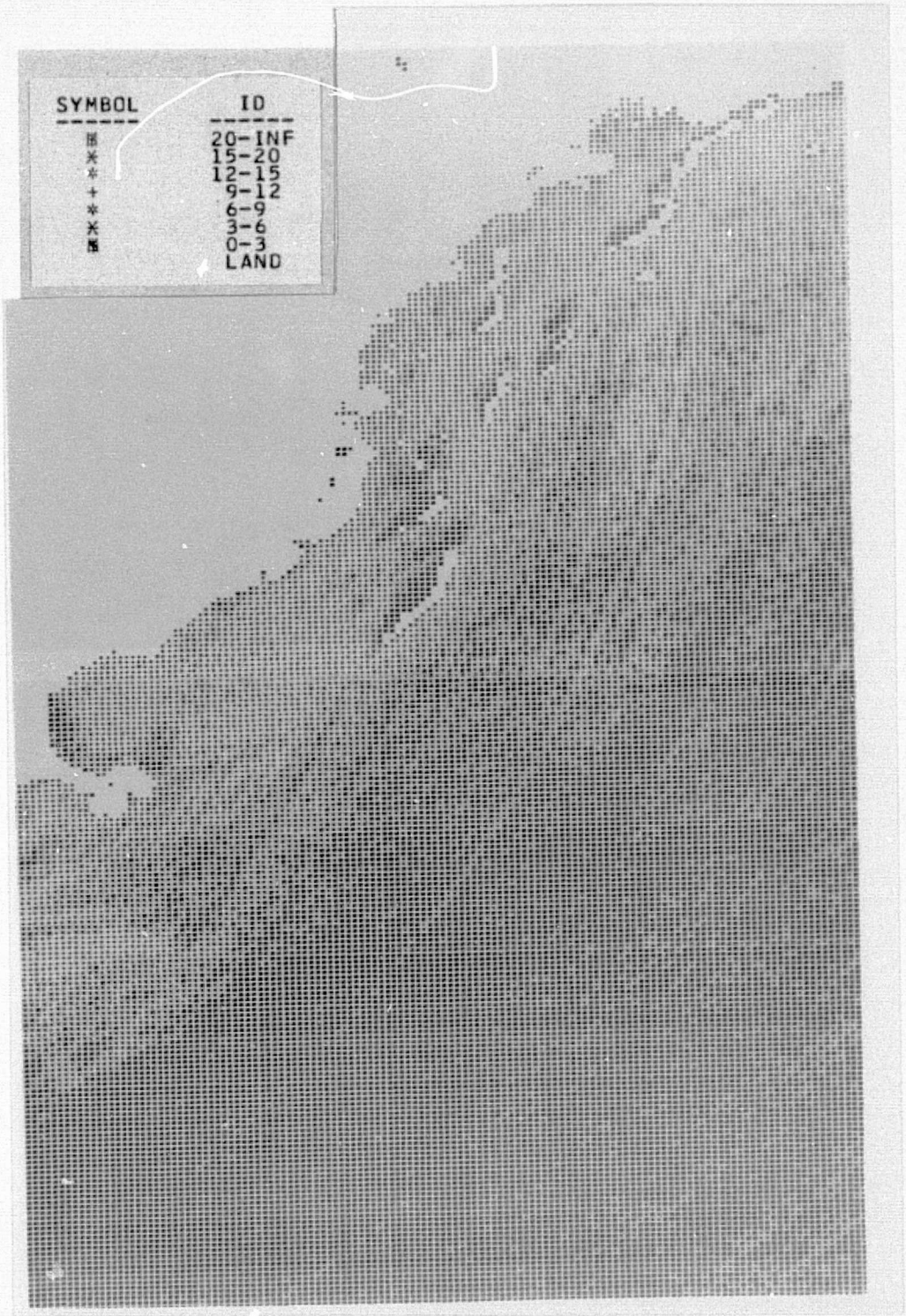

FIGURE 3. BATHYMETRIC CHART FOR SOUTHERN COAST OF PUERTO RICO, MADE FROM S-192 BAND 3

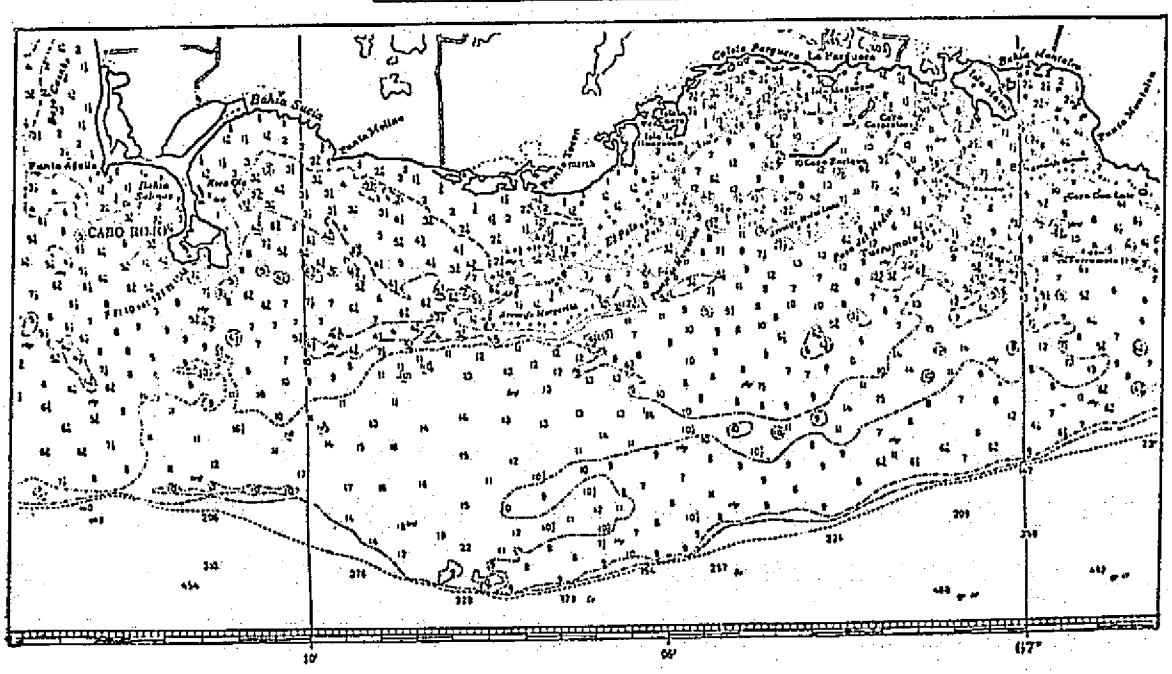

FIGURE 4. PORTION OF COAST AND GEODETIC SURVEY CHART 901, SHOWING SOUTHERN COAST OF PUERTO RICO

attempt was unsuccessful, and it was finally concluded that the anomalies were caused by ringing in the processed S-192 data. This ringing is clearly present in the processed S-192 imagery shown in Figure 2a and is not present in the S-190 photography. The anomalies always occur in the data immediately behind bright areas, such as Cabo Rojo and Arrecife Margarita, (scan lines run from lower left to upper right in the portion of the data shown in Figure 3).

Because of these data problems, no detailed analysis of the accuracy of the depth map (Figure 3) was attempted. However, the 8 fathom (15 meter) ledge southwest of Cabo Rojo can be seen on the depth map, indicating a substantial improvement over the 9 meter penetration depth reported for LANDSAT data [4].

3.1.2 WESTERN COAST

In September 1974, a set of data tapes was received for the same pass over Puerto Rico after undergoing revised signal processing procedures at Johnson Space Center. This set contained all 22 channels, and the noise in some of the channels (notably band 2) was less than that on the first tape received. The new tapes also contained data from about 10 seconds earlier, thus including parts of the western coast of Puerto Rico. This was important because the data collected just before the large could bank over Puerto Rico contains much less low-frequency noise then the subsequent data (apparently the noise was caused by the high signal received over the clouds).

After examining various parts of the data set it was decided to process the area off the West Coast of Puerto Rico. This area includes shallow water features (indicated as Escollo Negro on the Coast and Geodetic Survey Chart) and appears to have less noise than the southern coast data. A large part of the west coast is obscured by clouds and by a large dark plume extending outward from Mayaguez.

This plume has been tentatively identified as industrial waste products (possibly including fish oil and/or molasses) from plants near Mayaguez. Within the designated area, the plume follows the deep water boundary quite closely and, therefore, does not greatly affect the depth chart.

Processing of this area began by selecting a set of points where depths were indicated on Coast and Geodetic Chart 901. Data values in bands 2 and 3 at these points were then extracted from the tape. The deep water signal V_s was subtracted from each data value and the results plotted versus depth on semi-log paper (Figure 5). A linear regression analysis of this data yielded an attenuation coefficient of approximately 0.05 m^{-1} for both bands, in agreement with minimum oceanic values published in the Smithsonian Physical tables.

A digital depth chart was then produced for this area, using the optimum-decision-boundary techniques (Section 4 and Appendix) with the input parameters generated by the foregoing analysis. This chart is shown in Figure 6, where the symbols correspond to the depth ranges in Figure 3. The white area in the upper right-hand corner is the tip of Punta Guanajibo. A portion of Coast and Geodetic Survey Chart 901 covering the same area is reproduced as Figure 7.

Next, an accuracy check was made by comparing depth values calculated by the optimum-decision-boundary technique with values read from the Coast and Geodetic Survey Chart. Both sets of values are plotted in Figure 8 along line 1450 taken from the digital depth map. The root-mean-square difference between the calculated and chart values along this line is approximately 2.4 meters. Subsequently, a depth transect corresponding to line 1440 was also received from J.V.A. Trumbull [5] of the U.S. Geological Survey. A portion of this transect is plotted, along with the calculated values, in Figure 9. The r.m.s.

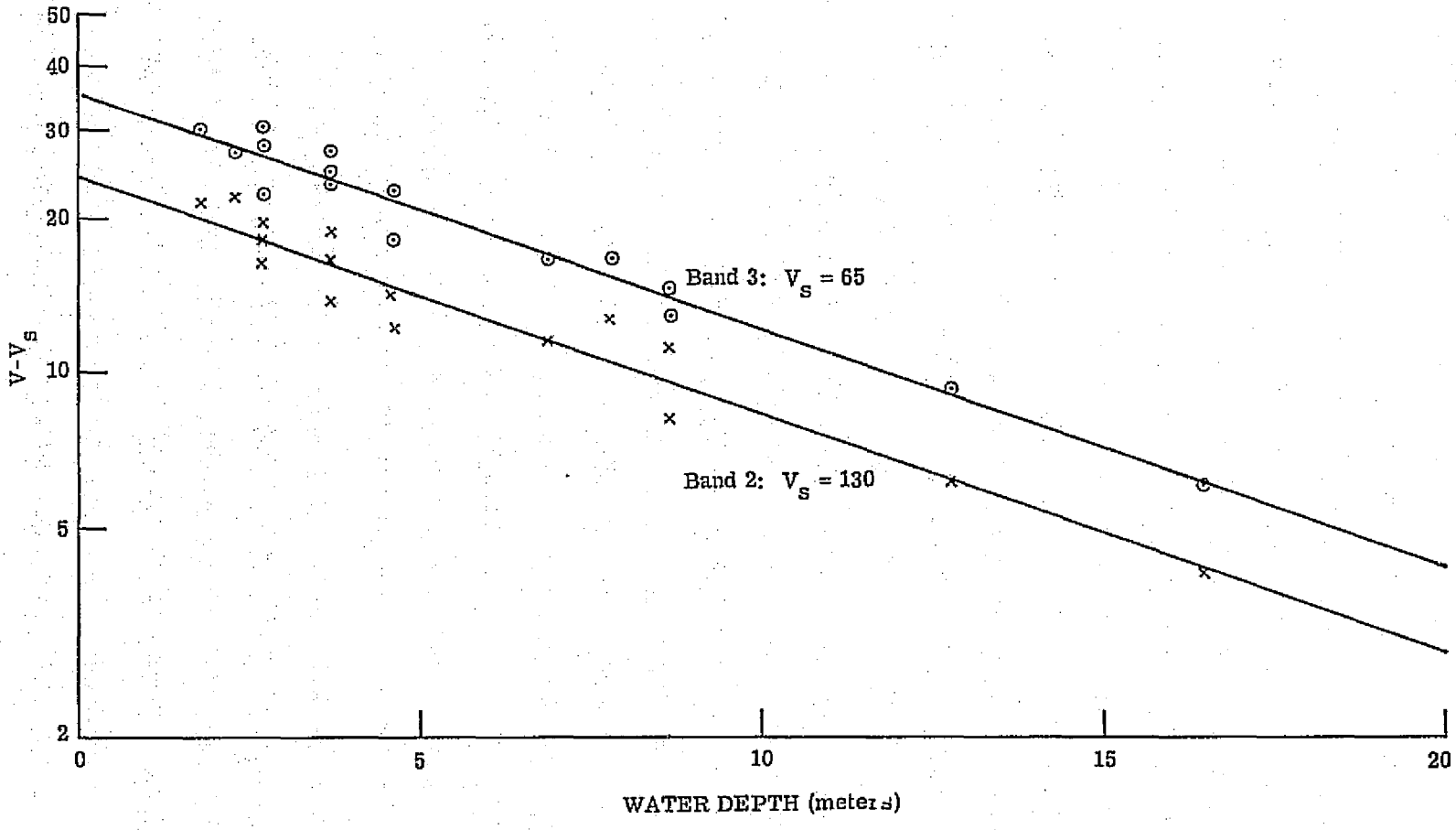

FIGURE 5. S-192 BAND 2 AND 3 SIGNALS VERSUS DEPTH, ESCOLLO NEGRO AREA
(PASS 6 - JUNE 9, 1973)

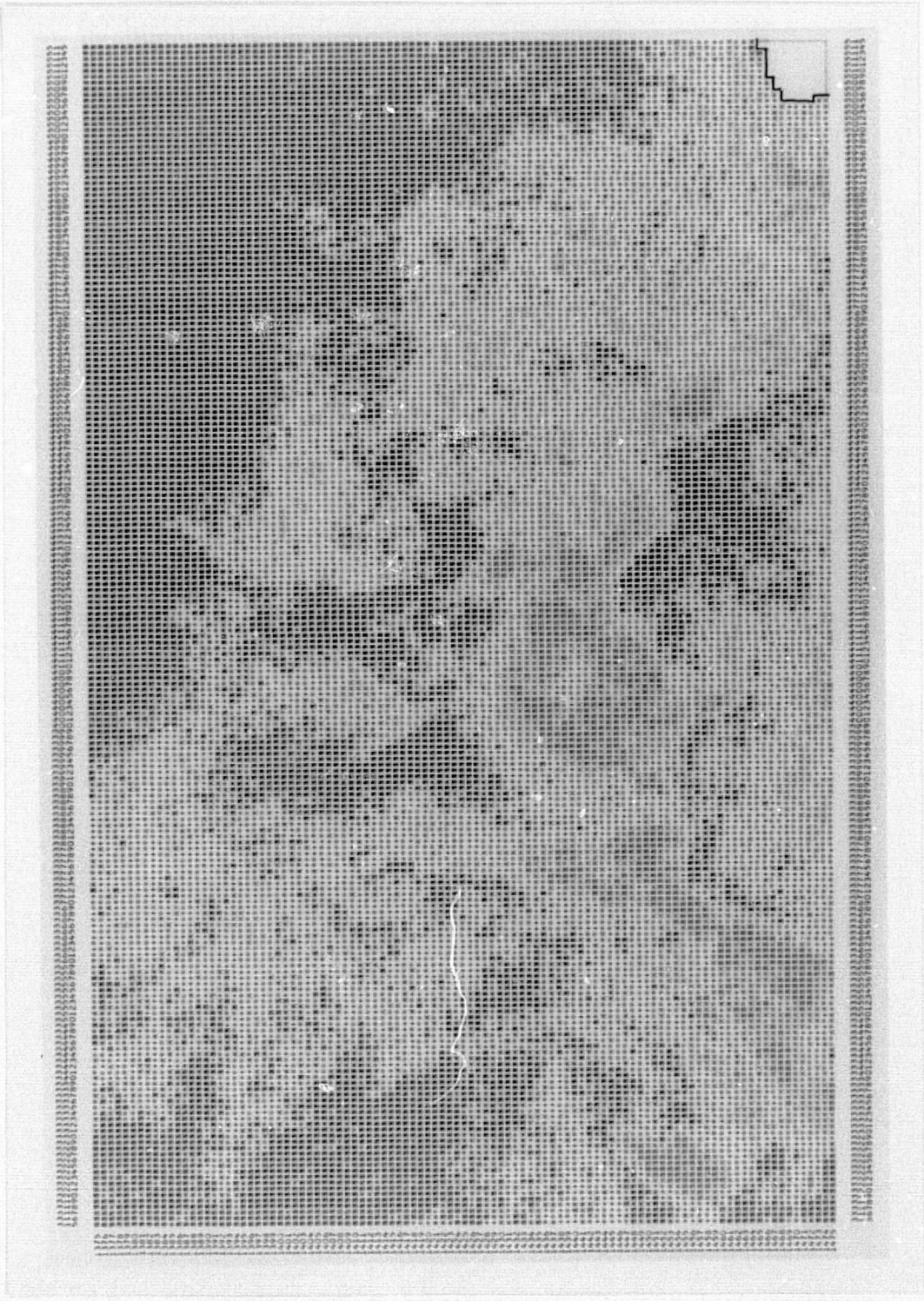

FIGURE 6. BATHYMETRIC CHART FOR WESTERN COAST OF PUERTO RICO, MADE FROM S-192 BAND 2 AND 3

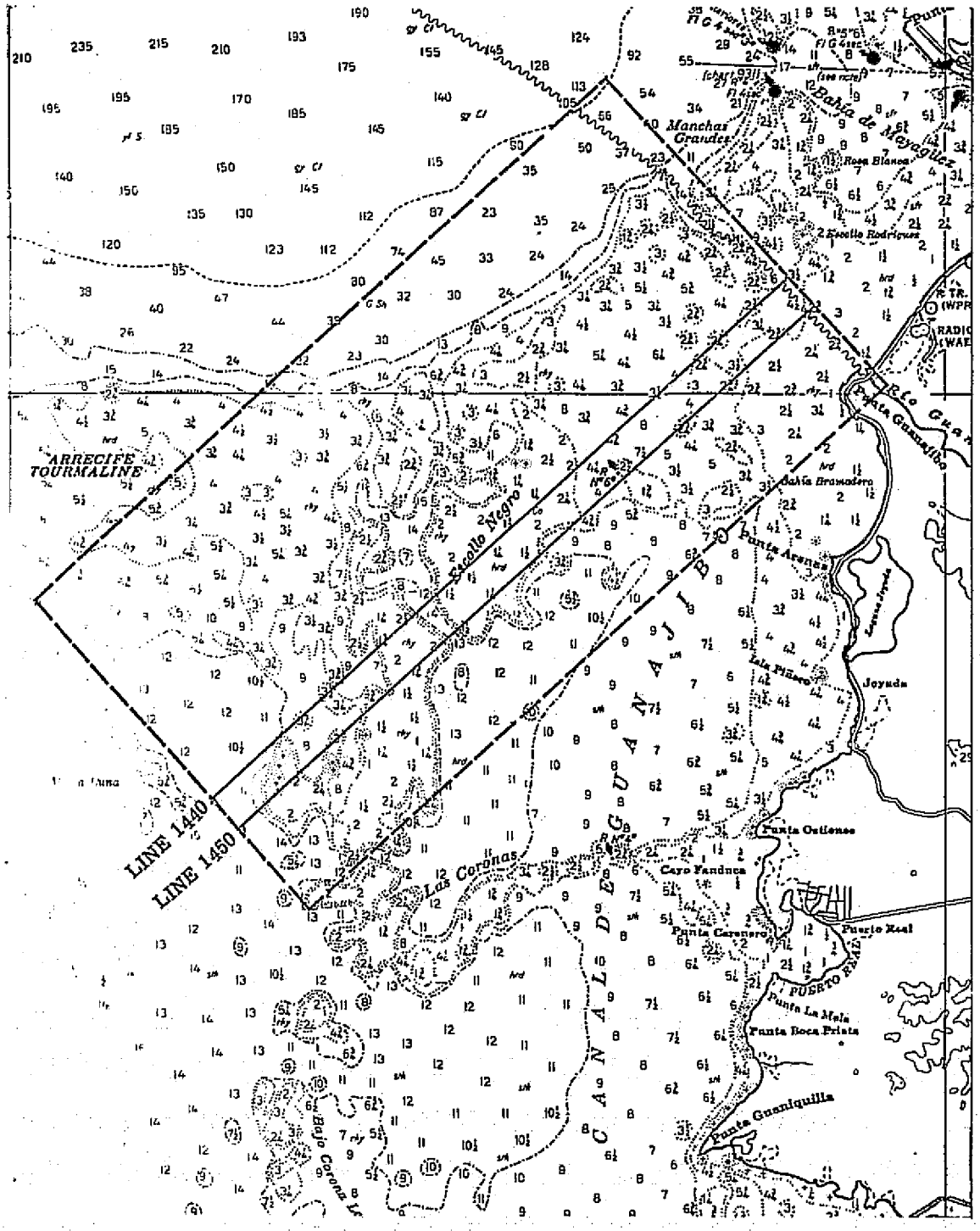

FIGURE 7. PORTION OF C&GS CHART 901, WESTERN COAST

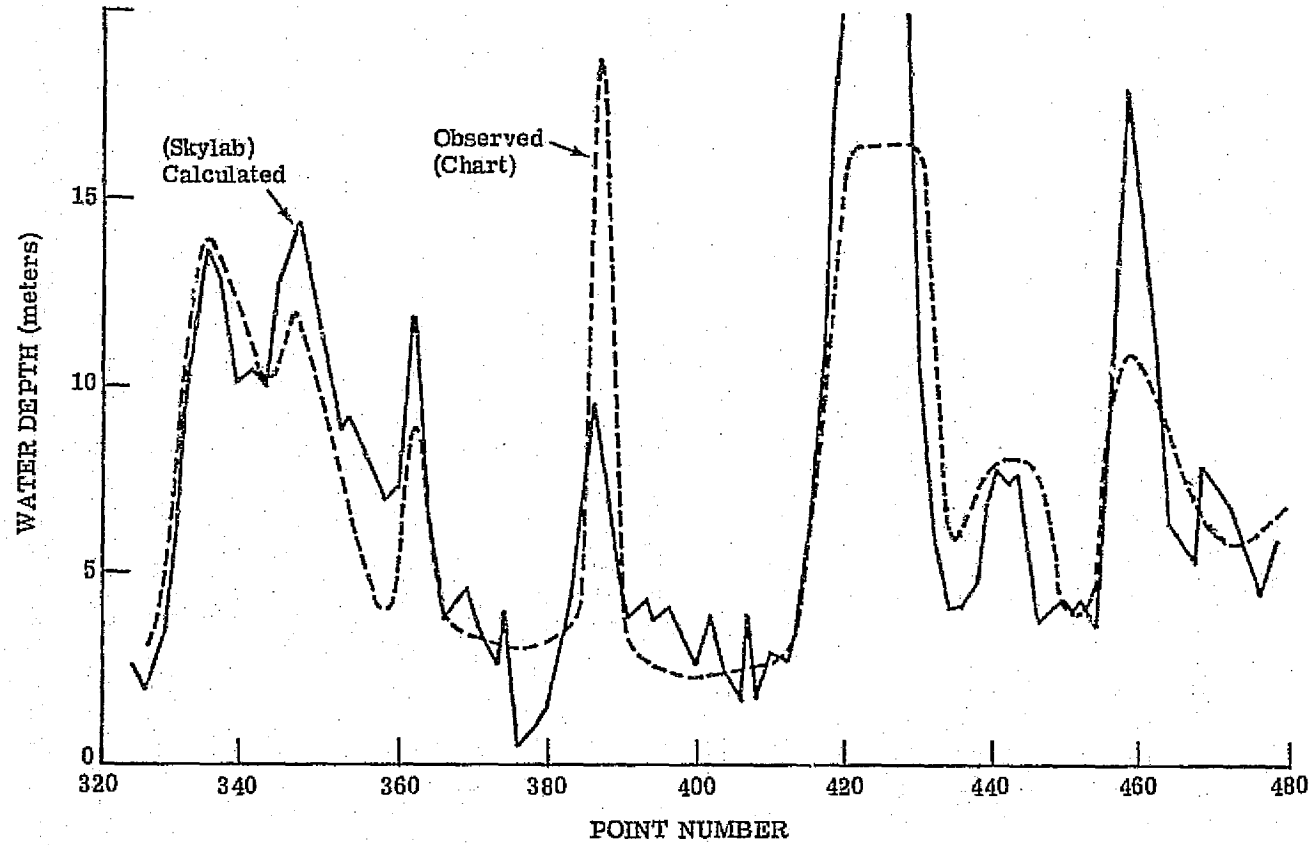

FIGURE 8. CALCULATED AND CHART DEPTHS ALONG LINE 1450 (ESCOLLO NEGRO)

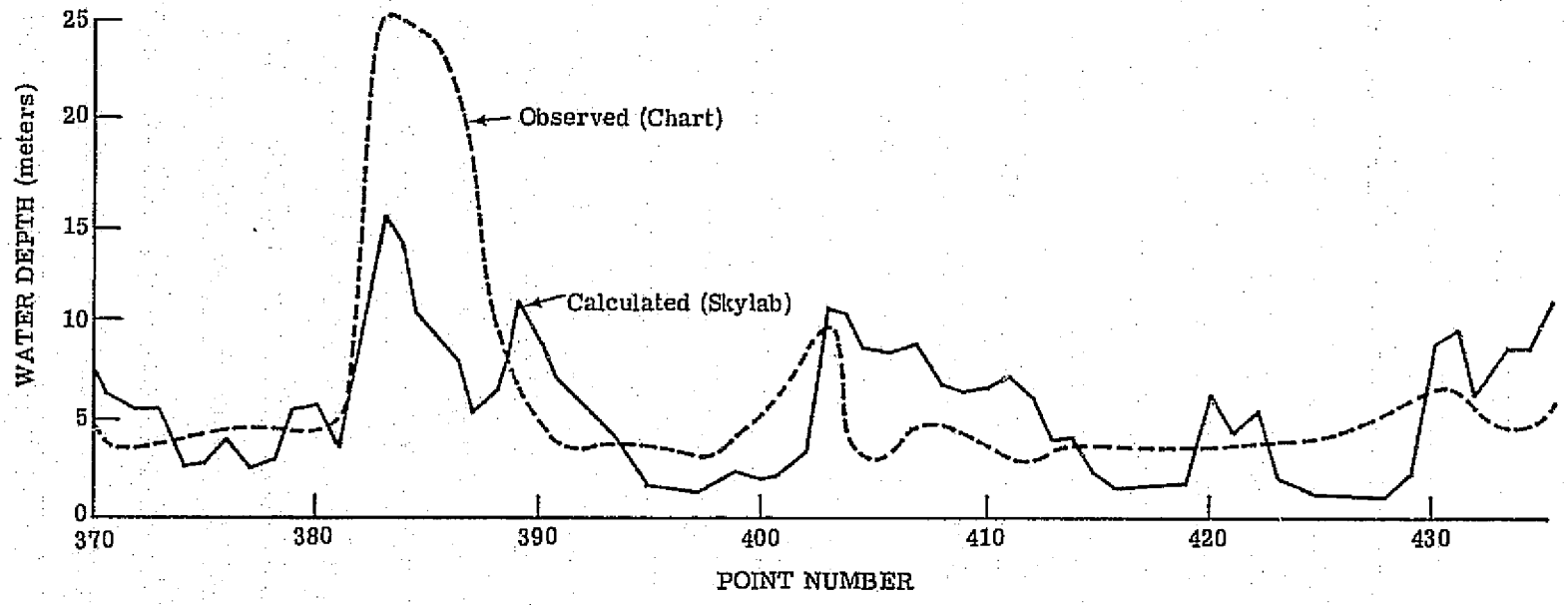

FIGURE 9. CALCULATED AND CHART DEPTHS ALONG LINE 1440 (ESCOLLO NEGRO)

difference between the calculated and observed values along this line is approximately 3.8 meters.

The greatest difference between calculated and observed depths occurs in the narrow channel running through the Escollo Negro (at approximately point 384 in Figures 8 and 9). Neglecting the possibility that this channel has actually filled in since the depth measurements were made, the error here is probably due to slow time-response characteristics of the S-192 sensor. Calculated depths in the Canal de Guanajibo are also smaller than the measured values. This difference is perhaps due to an increased surface-reflected signal due to nearby clouds. Other sources of error include changes in the surface-reflected signal due to sea-state conditions, and changes in water quality or bottom reflectance.

Errors due to changes in water quality or bottom reflectance can be minimized by the use of the ratio method [4], but only at the expense of increased error due to changes in the surface-reflected signal. For the present case, the minimum overall error was obtained by the use of the optimum-decision-boundary technique, chiefly because of the relatively poor data quality in the red band (band 5) which is used in the ratio method. A more complete discussion of the errors inherent in each depth calculation technique is included in the Appendix.

The calculation of depth accuracy is hampered by lack of precise knowledge of the location of the depth transects. In addition, some discrepancy is expected due to the difference between the area resolution of Skylab data and that of the sonar data which was used in compiling the Coast and Geodetic Survey chart. Furthermore, Coast and Geodetic Survey data were taken at a different time than Skylab overpass and some bottom changes due to currents, wave action, and growth of sand bars may have occurred.

There is need for a well conducted experiment where depths are obtained simultaneously with the overpass of the satellite and the position accuracy of the depths measured can be accurately related to the pixel elements of the MSS image as stored in the CCT's for the scene.

3.2 PASS 14: CENTRAL LAKE MICHIGAN SHORELINE

In order to test the technique under a variety of water transparency conditions, a second test site was chosen where the attenuation was greater than that encountered near Puerto Rico.

Data tapes from Skylab-3 pass 14 over Lake Michigan were received at ERIM in October 1974. Data was taken over the eastern shore of Lake Michigan during this pass at 15:01:30 GMT on 5 August 1973. Skies were clear over the Michigan shoreline and the solar zenith angle was approximately 45°. The S-190B photography and screening films for this area are shown in Figures 10 and 11a and b.

Notable features on the lake include a white streak along the shoreline on the lower half of the frame. This streak bears a striking resemblance to clouds on the S-190B photography, but its absence on the thermal imagery (Figure 11b reveals it to be a sediment plume in the water.

Very little shallow water is visible in the scene because of the rapid drop-off in water depth along the shoreline. However, an enlargement of S-190B photography (Figure 12) of the shoreline near Pentwater, at the center of the frame, shows a series of two or three sand bars parallel to the shore. The water seems to be fairly clean in this area because of its protected position between Big Sable Point (to the north) and Little Sable Point (to the south).

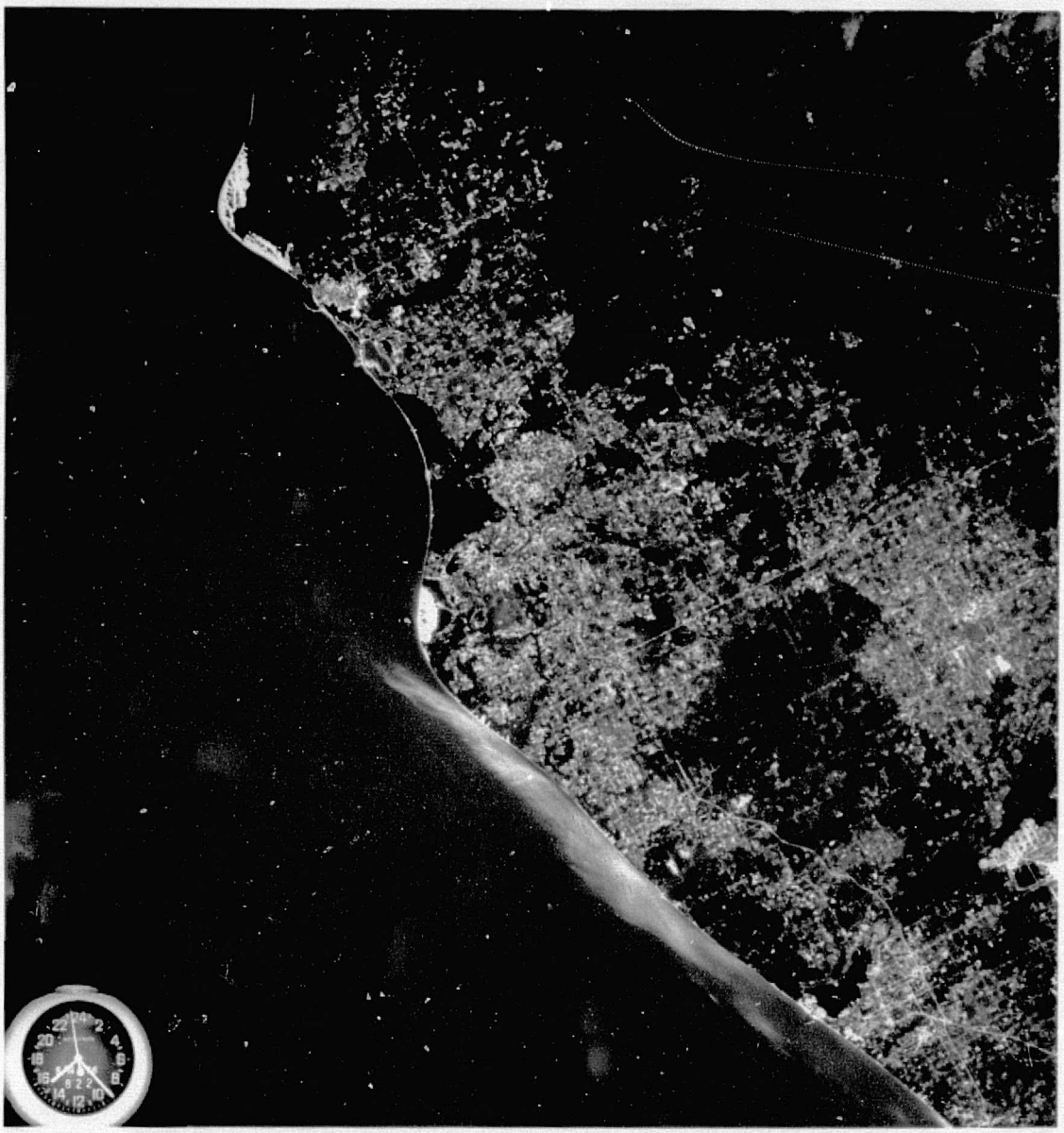

FIGURE 10. S-190B PHOTOGRAPH OF EASTERN LAKE MICHIGAN (PASS 14 - AUGUST 5, 1973)

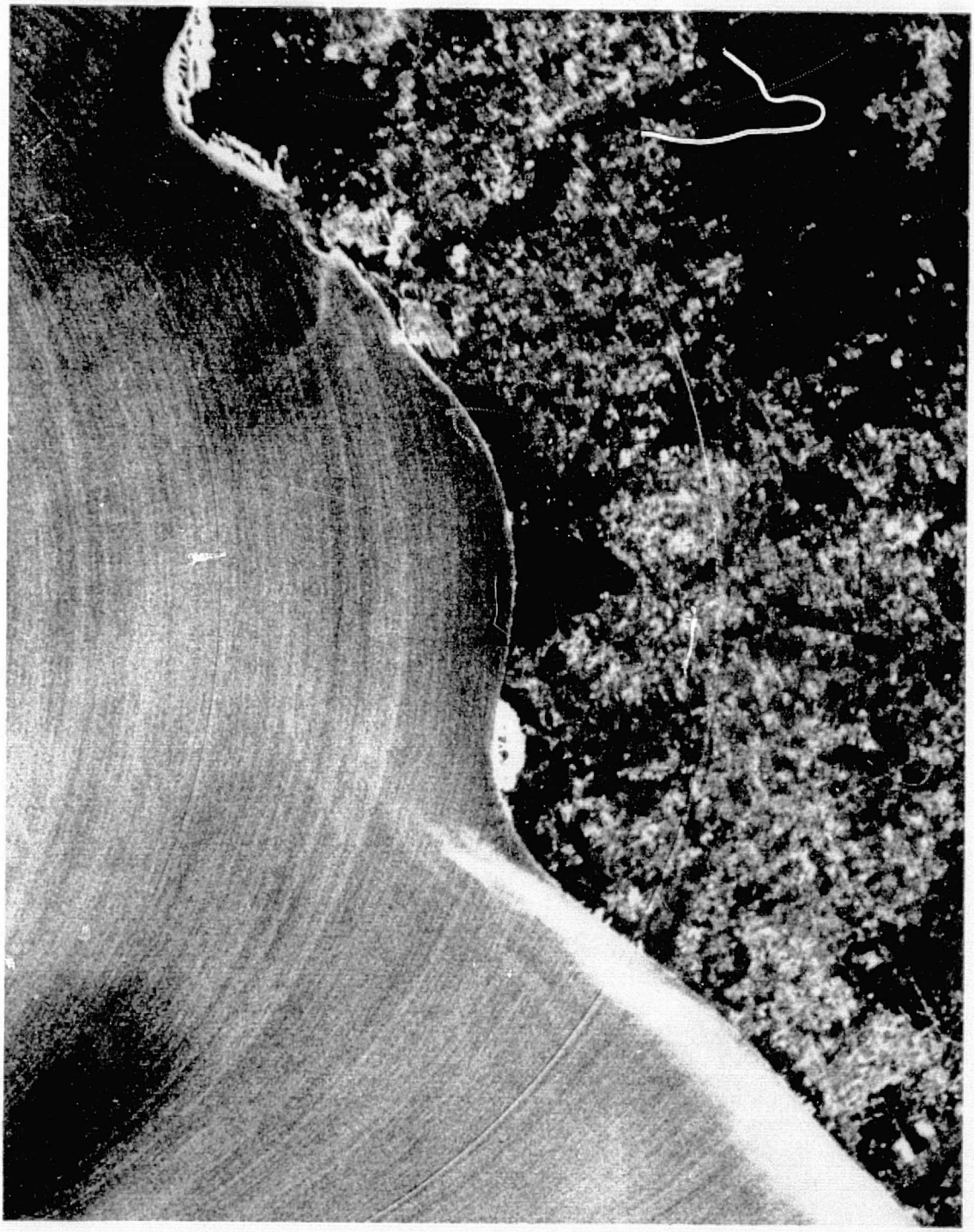

FIGURE 11a. PROCESSED IMAGERY FOR S-192 EASTERN LAKE MICHIGAN
(PASS 14 - AUGUST 5, 1973) BAND 3: 0.50-0.55 μm

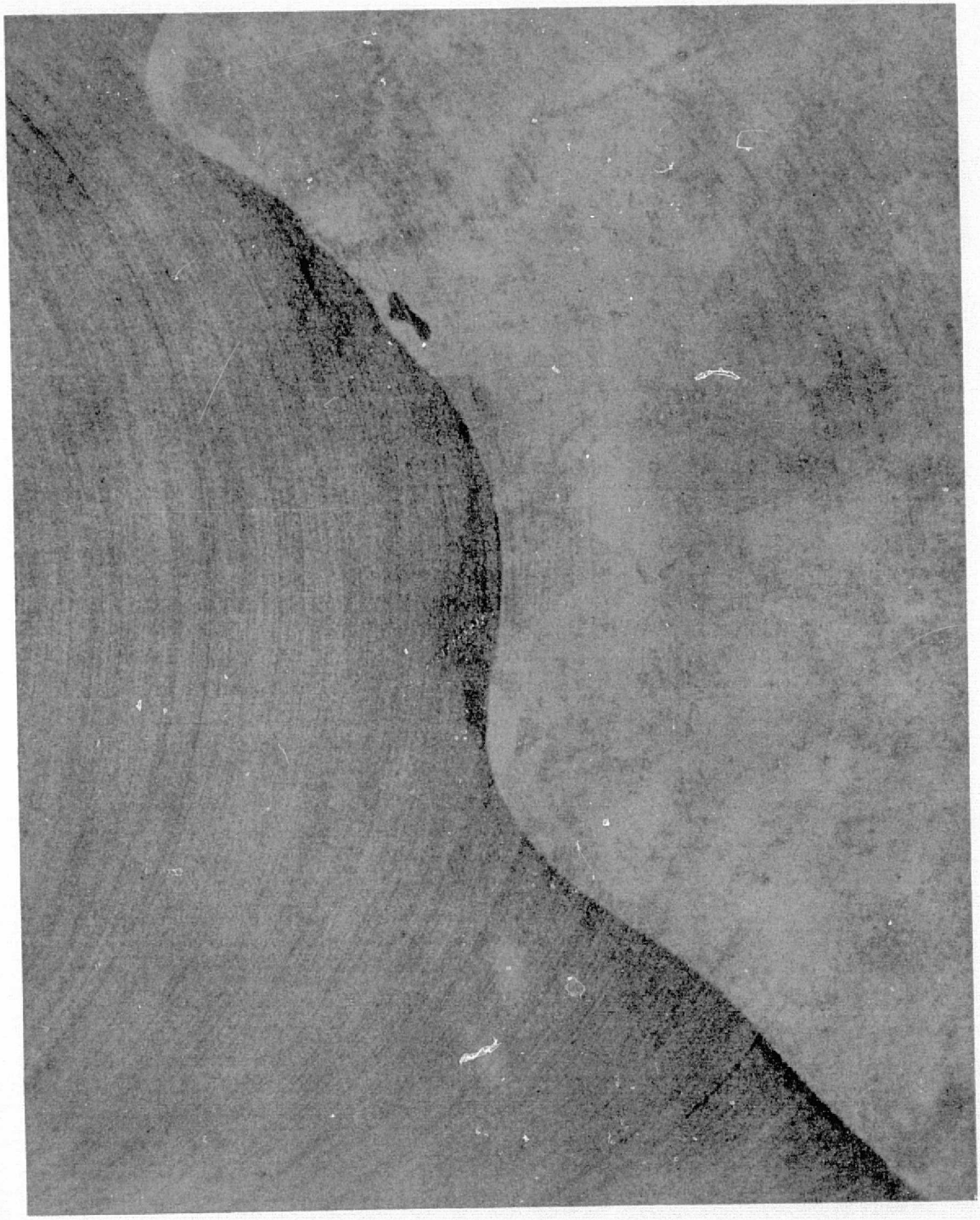

FIGURE 11b. PROCESSED IMAGERY FOR S-192 EASTERN LAKE MICHIGAN (PASS 14 - AUGUST 5, 1973) BAND 13: 10.2-12.5 μm

FIGURE 12. ENLARGEMENT OF S-190B PHOTOGRAPH SHOWING MULTIPLE SAND BAR STRUCTURE ALONG THE MICHIGAN COASTLINE

These sand bars have dimensions only slightly larger than the S-192 pixel size (determined as 70 meters by a comparison of line and point numbers with a topographic map), so they are not resolved consistently in the scanner data. At certain locations, however, evidence of the sand bars can be seen in the scanner data by averaging several pixels together parallel to the shoreline. This was done for a transect approximately 1 mile south of Pentwater, Michigan, where the scan lines happened to be exactly parallel to the shoreline. Scene points 535 through 538 were averaged together on a line-by-line basis for lines 3577 through 3590 in bands 3 and 4 of the S-192 data. The results, plotted in Figure 13, show a peak signal at lines 3579, 3582, and 3584. These are at distances of approximately 560, 350, and 210 meters, respectively, from the shoreline (line 3587).

In order to confirm these distances, the S-190B photographic transparency was examined using a Jarrell-Ash scanning densitometer. The instrument was set to scan along the same transect south of Pentwater, at a rate of 1 millimeter per minute. The aperture was set at a size equivalent to .015 mm by .125 mm on the film, the longer dimension being perpendicular to the scan direction. This corresponds to a spot size of approximately 14.5 by 120 meters on the ground (the scale of the transparency was found to be 1:967,000 by direct measurement and comparison with the topographic map). The output from the densitometer, in units proportional to the film transmission, was recorded on a strip chart moving at 3 inches per minute. Each half-inch division on the chart thus corresponds to a ground distance of about 160 meters (same horizontal scale as Figure 13).

The densitometer scan (Figure 14) shows three peaks at locations corresponding very closely to the peaks in the S-192 data. Assuming these are sand bars, the water depth can be calculated at each sand bar if the water attenuation coefficient is known. Unfortunately, no

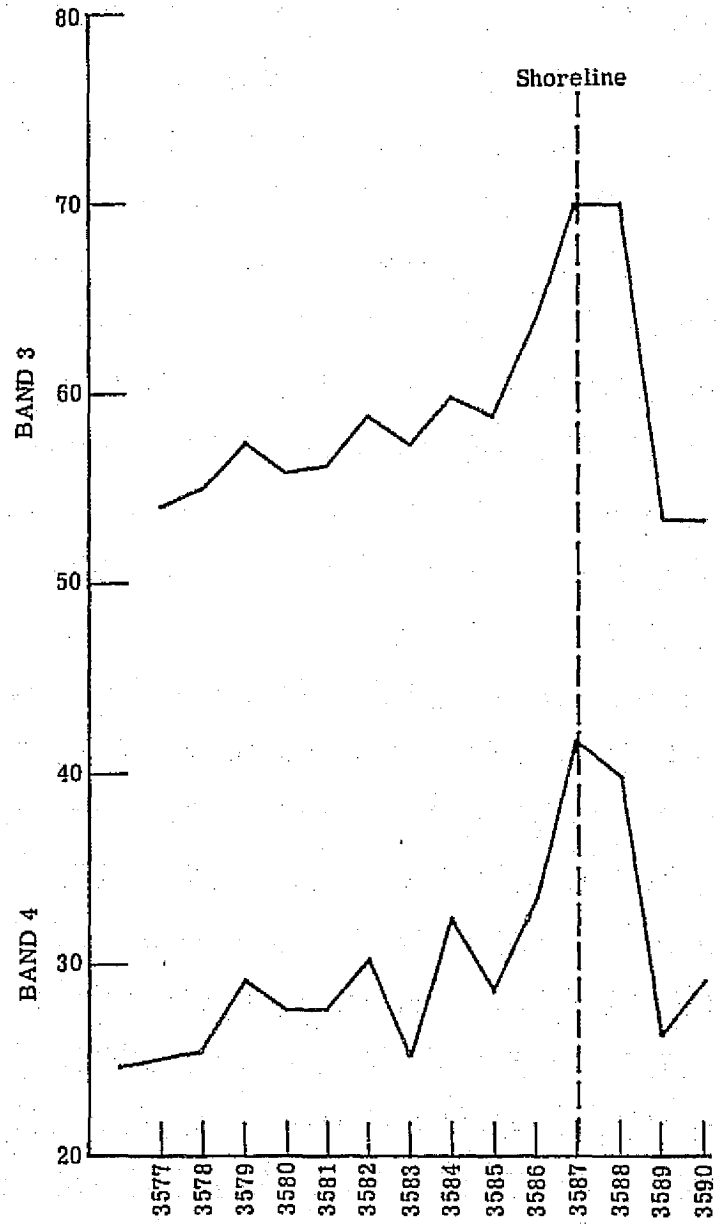

FIGURE 13. S-192 BAND 3 AND 4 DATA VALUES VERSUS LINE NUMBER FOR TRANSECT PERPENDICULAR TO SHORELINE 1 MILE SOUTH OF PENTWATER, MICHIGAN

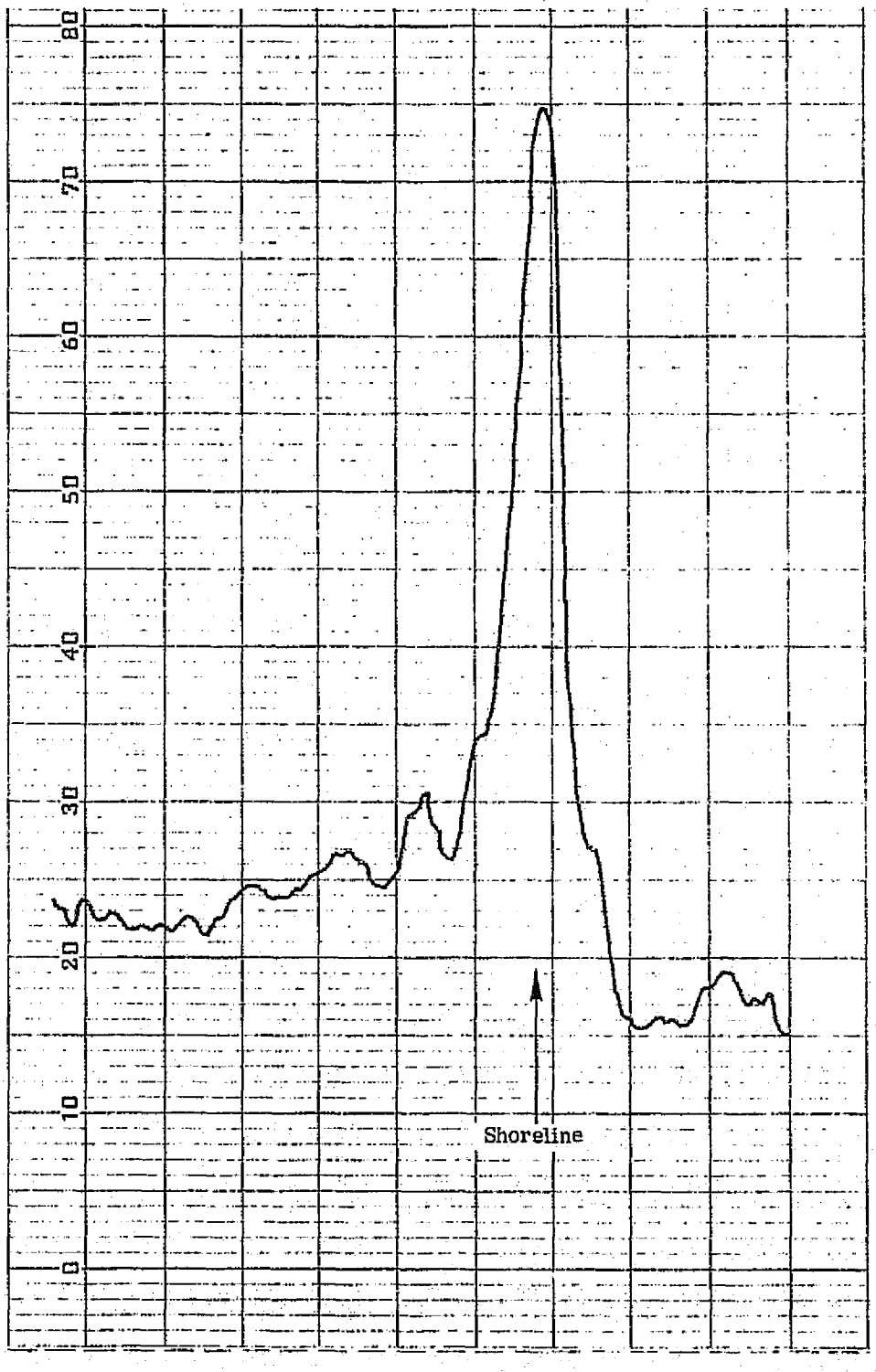

FIGURE 14. S-190 FILM DENSITY VERSUS DISTANCE FROM SHORELINE FOR THE SAME TRANSECT AS IN FIGURE 13

ground truth data was collected at this time of the overflight. However, an estimate can be made by using the attenuation coefficient $\alpha = .055\ ft^{-1}$ reported by Brown et al. [3] for Lake Michigan water at the wavelengths corresponding to band 3. The equation relating signal to depth is:

$$V = V_s + V_o\, e^{-\alpha f z}$$

where V = signal at depth z in band 3

V_s = signal over deep water ($z = \infty$)

V_o = bottom-reflected signal at shoreline ($z = 0$)

α = water attenuation coefficient

$f = \sec\theta + \sec\phi$

θ = scan angle (under water)

ϕ = solar zenith angle (under water)

Using the observed values $V_s = 55$, $V_o = 15$, and $f = 2.42$ from the S-192 data, the depths calculated for each sand bar are 13.4 ft., 10.0 ft., and 8.3 ft., respectively.

No direct depth measurements were made in this area at the time of the overflight. However, sand bars are common in this area, and Lake Survey Chart 77 shows two sand bars south of Pentwater (Figure 15), at distances of about 210 and 360 meters from shore. The depths are indicated as about 6 and 10 ft., respectively, in fair agreement with the calculated depths. No third sand bar is shown on the Lake Survey Chart, but its existence is possible since they are known to form and disappear quite rapidly due to wave action.

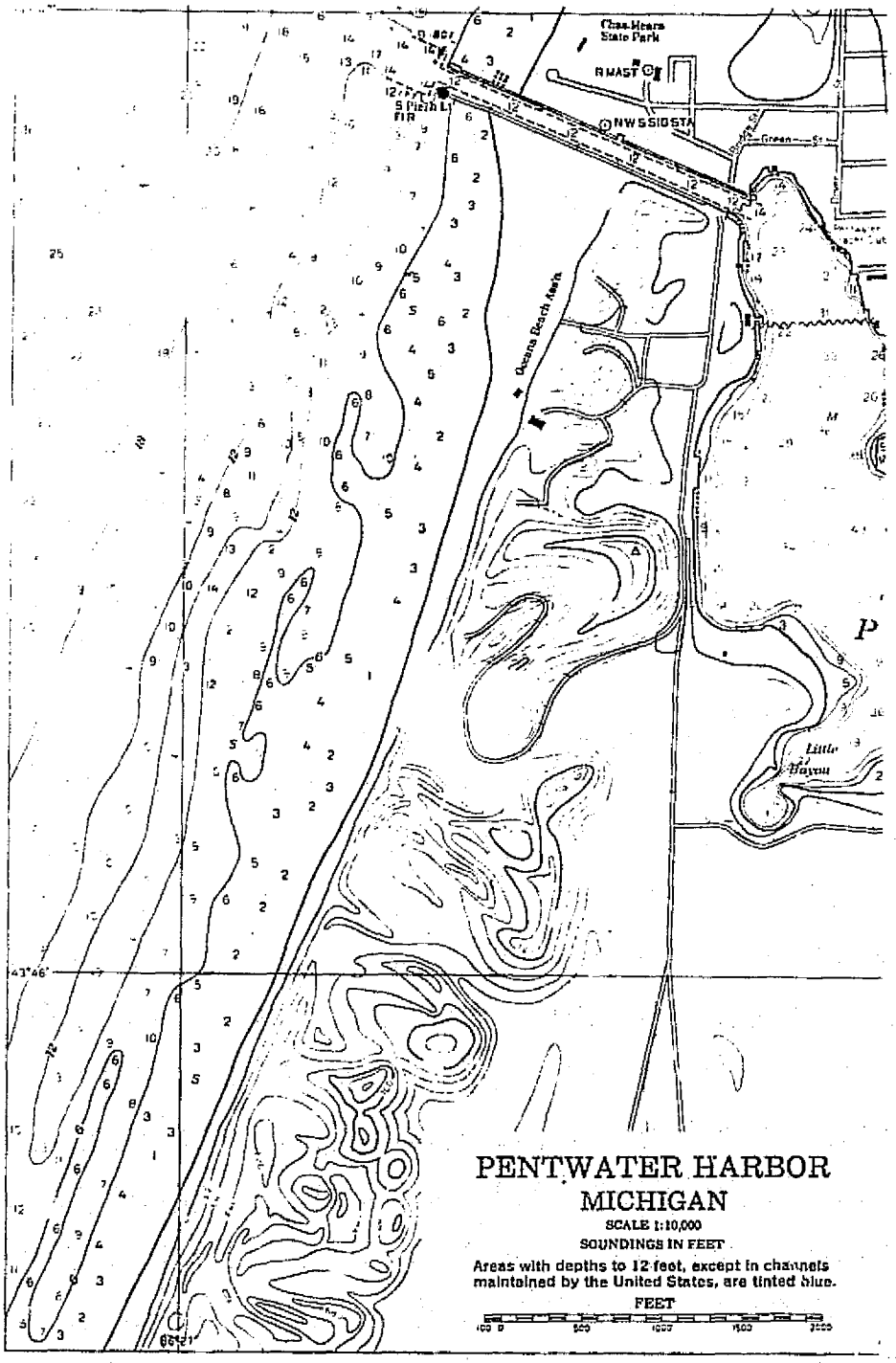

FIGURE 15. PORTION OF LAKE SURVEY CHART 77, SHOWING LAKE MICHIGAN SHORELINE NEAR PENTWATER, MICHIGAN

3.3 PASS 54: EASTERN PUERTO RICO

3.3.1 ESCOLLO de ARENAS

In the Lake Michigan data set, the high-resolution S-190B photography was used to confirm the presence of very small features just marginally within the resolution capability of the S-192 scanner. An opportunity to attempt to use the photography in a more quantitative fashion was provided by a second data set collected over Eastern Puerto Rico during Skylab Pass 54.

Skylab-4 passed over the southeast corner of Puerto Rico at 16:43:30 GMT on 30 November 1973. The solar zenith angle was approximately 42° and skies were partly cloudy. Some shallow water features are visible on the photography (Figure 16) and screening film (Figure 17), the most prominent being a long narrow shoal extending upward from the west end of Isle de Vieques. This shoal, the Escollo de Arenas, is indicated on Coast and Geodetic Survey Chart 904 (Figure 18), although with a slightly different shape. The minimum depth indicated on the chart is approximately 2.5 meters.

In order to compare water depths with S-192 data values and S-190B film density, a transect was drawn through the center of Escollo de Arenas and depths were read along this transect from the Coast and Geodetic Survey Chart. The results are plotted in Figure 19 (top curve) at a scale of approximately 1.6 km per inch. Data values along lines 2184 and 2185 of the scan line-straightened S-192 data (band 3) were then read from the magnetic tape on ERIM's PDP-8 computer. These two lines were averaged together on a point-by-point basis from points 900 to 1030 and plotted in Figure 19 (center curve) at a scale of 25 points per inch.

Finally, the S-190B photographic transparency was placed in the Jarrell-Ash densitometer and the same transect was scanned at 5 mm/min with the aperture set at .025 x .125 mm. In order to make the best

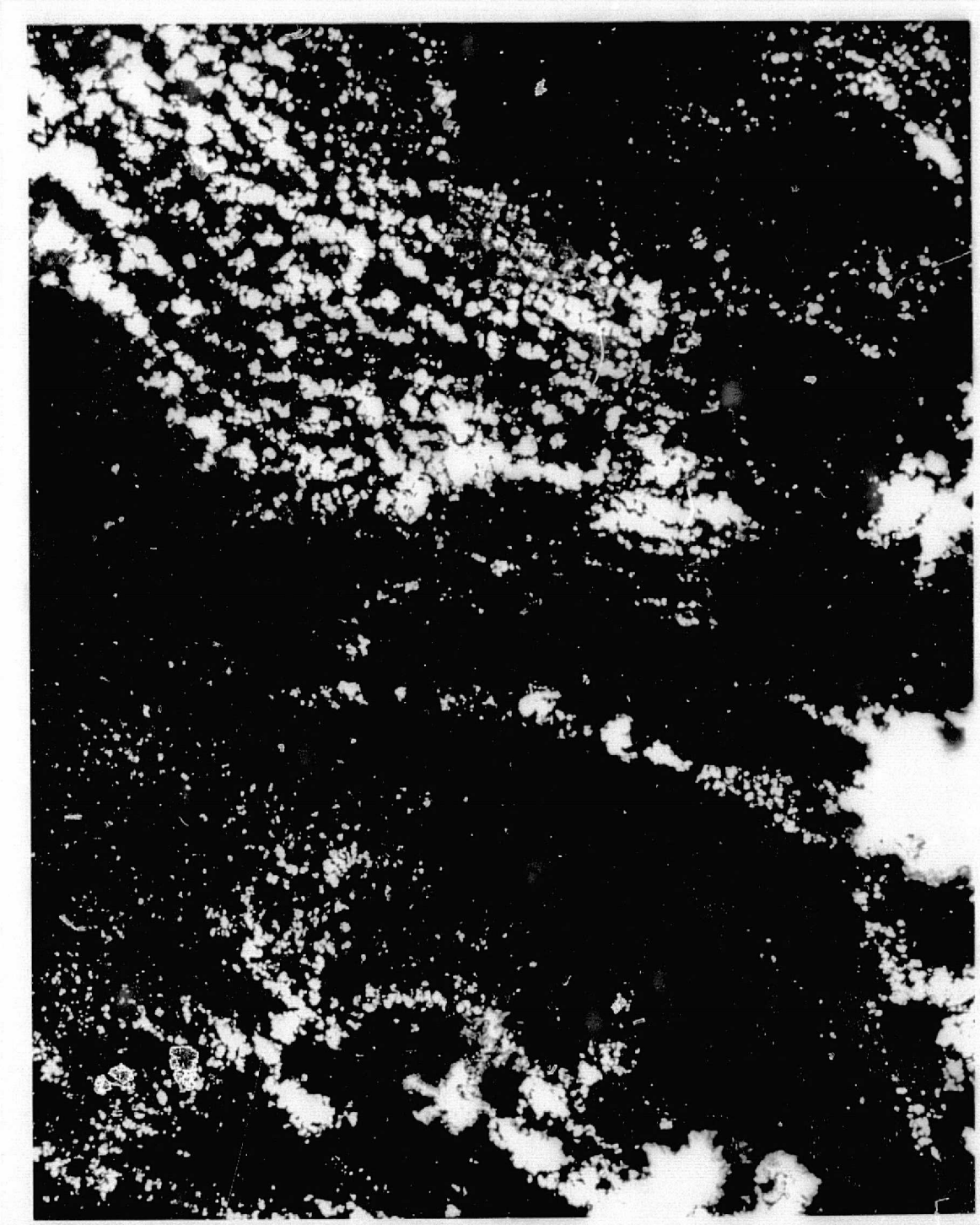

FIGURE 16. S-190B PHOTOGRAPH OF EASTERN PUERTO RICO
(PASS 54 - NOVEMBER 30, 1973)

FIGURE 17. PROCESSED S-192 IMAGERY FOR EASTERN PUERTO RICO
(PASS 54 - NOVEMBER 30, 1973 BAND 2, 45-50 μm)

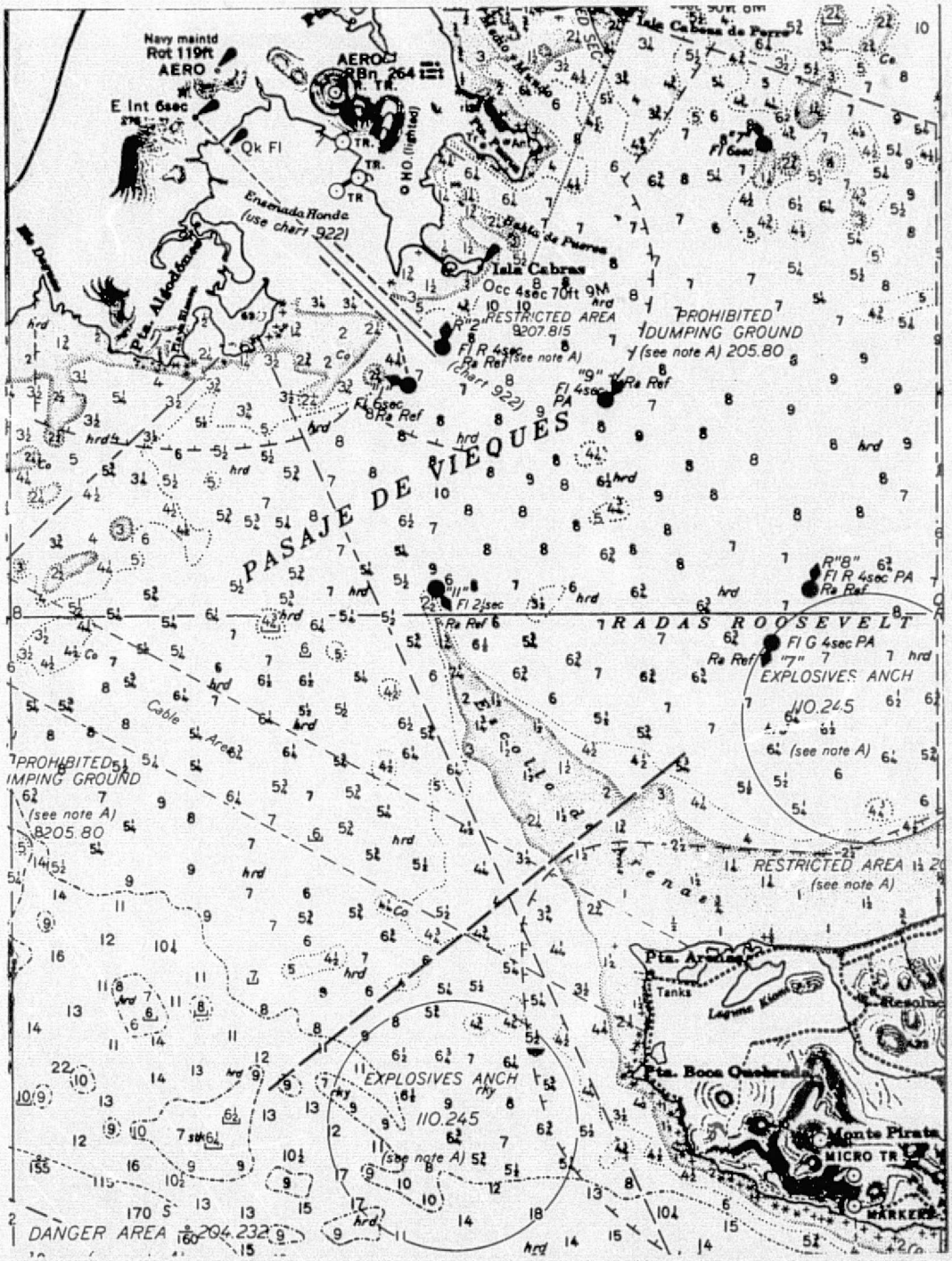

FIGURE 18. PORTION OF COAST AND GEODETIC SURVEY CHART 904, SHOWING ESCOLLO de ARENAS

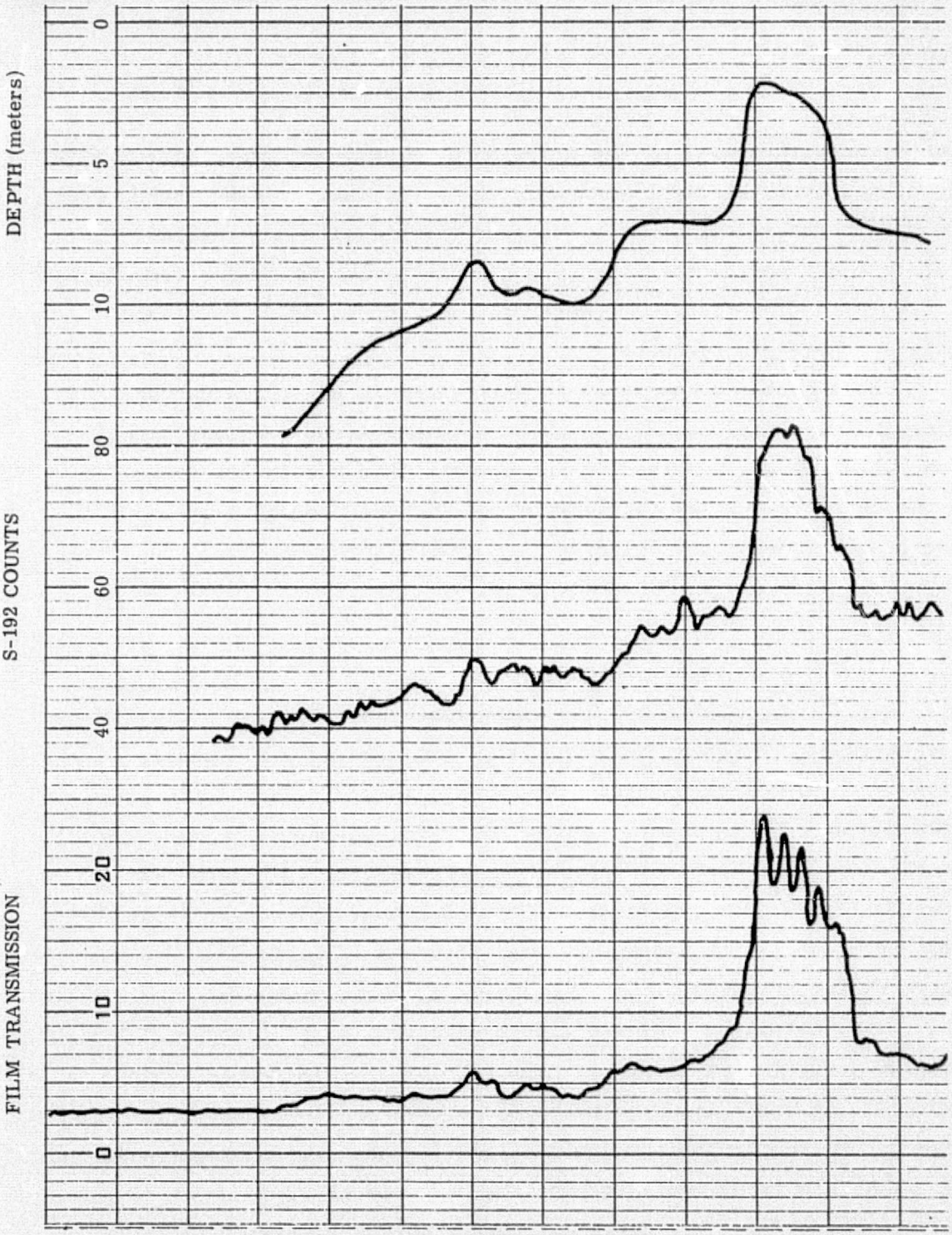

FIGURE 19. COMPARISON OF WATER DEPTH (TOP CURVE), S-192 DATA VALUES (CENTER CURVE), AND S-190B FILM DENSITY (LOWER CURVE) FOR TRANSECT THROUGH THE ESCOLLO de ARENAS. (PASS 54 - NOVEMBER 30, 1973)

comparison with band 3 of the S-192 data, a standard green filter (#58) was placed over the light source in the densitometer. The output from the densitometer, expressed as percent transmission, was recorded on a strip chart moving at 3 inches/min. The resulting trace, reproduced in Figure 19 (lower curve), therefore, has approximately the same scale as the depth transect.

Most features appear to be correlated in all three curves, although the densitometer scan shows a banded structure inside the shoal which is not resolved in the scanner data and is not indicated on the depth chart. An approximate relationship among water depth, band 3 data values, and filtered film transmission obtained from this comparison is shown in Table 1.

3.3.2 AVES (BIRD) ISLAND

Although the S-192 scanner was turned off shortly after passing Isle de Vieques, S-190 coverage extended several hundred kilometers further southeast. Aves (Bird) Island, which is located approximately 330 km southeast of Puerto Rico in the Caribbean, was covered on S-190B frame 90-066. An enlargement of this frame is shown in Figure 20. A portion of Naval Oceanographic Chart 25161, compiled from British surveys between 1840 and 1850, is shown in Figure 21 for comparison.

A densitometer scan was also made across Aves Island at 1.5 mm/min with the green filter in place. The results of this scan are shown in Figure 22. A shelf (light blue tone) is observed to extend nearly one kilometer to the southwest of the island (to the left on Figures 20 and 22). The film transmission at the edge of this shelf is about 10 percent, corresponding to a depth of about 6 meters according to Table 1.

TABLE 1

WATER DEPTH VERSUS BAND 3 DIGITAL DATA VALUES AND FILM TRANSMISSION

DEPTH (m)	BAND 3	PERCENT TRANSMISSION
3	80	20
5	65	12
7	55	7
10	48	5
∞	40	3

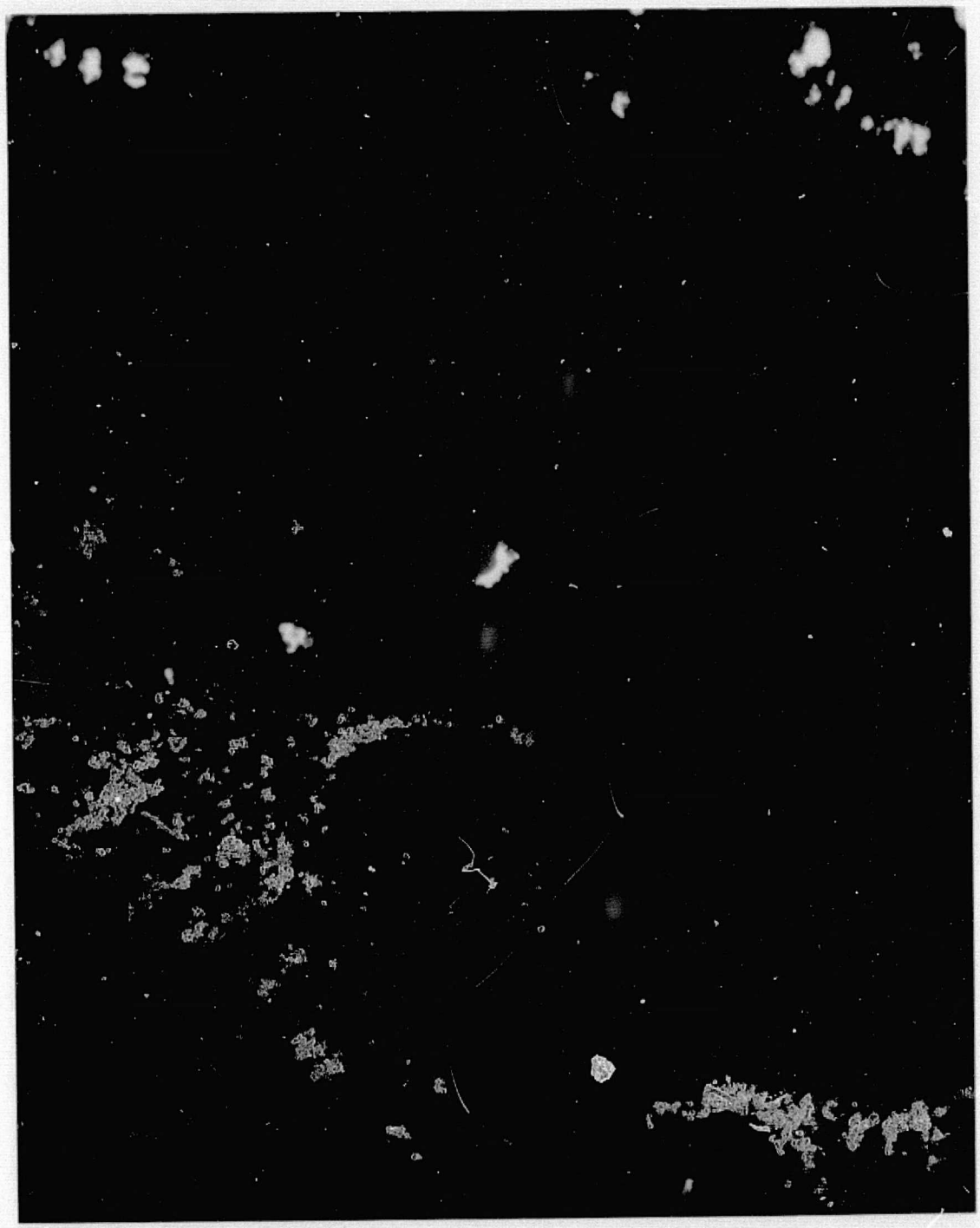

FIGURE 20. ENLARGEMENT OF S-190B PHOTOGRAPH SHOWING AVES (BIRD) ISLAND (PASS 54 - NOVEMBER 30, 1973)

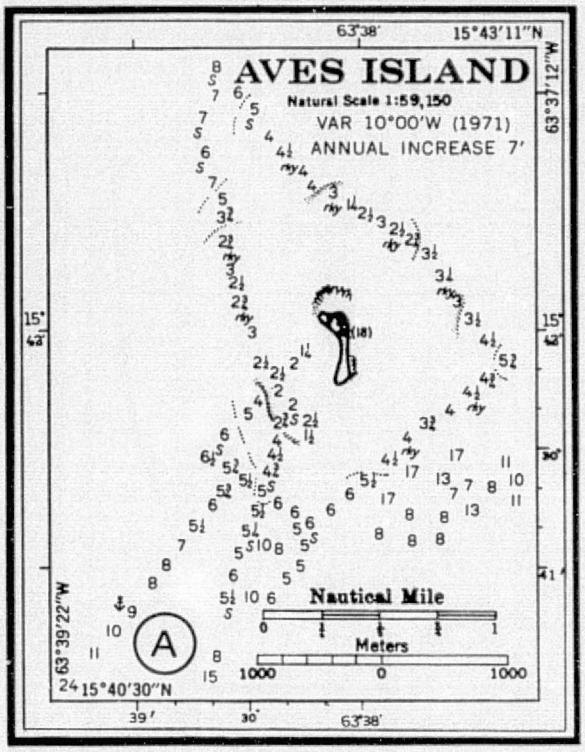

FIGURE 21. PORTION OF NAVAL OCEANOGRAPHIC CHART 2551, SHOWING AVES (BIRD) ISLAND

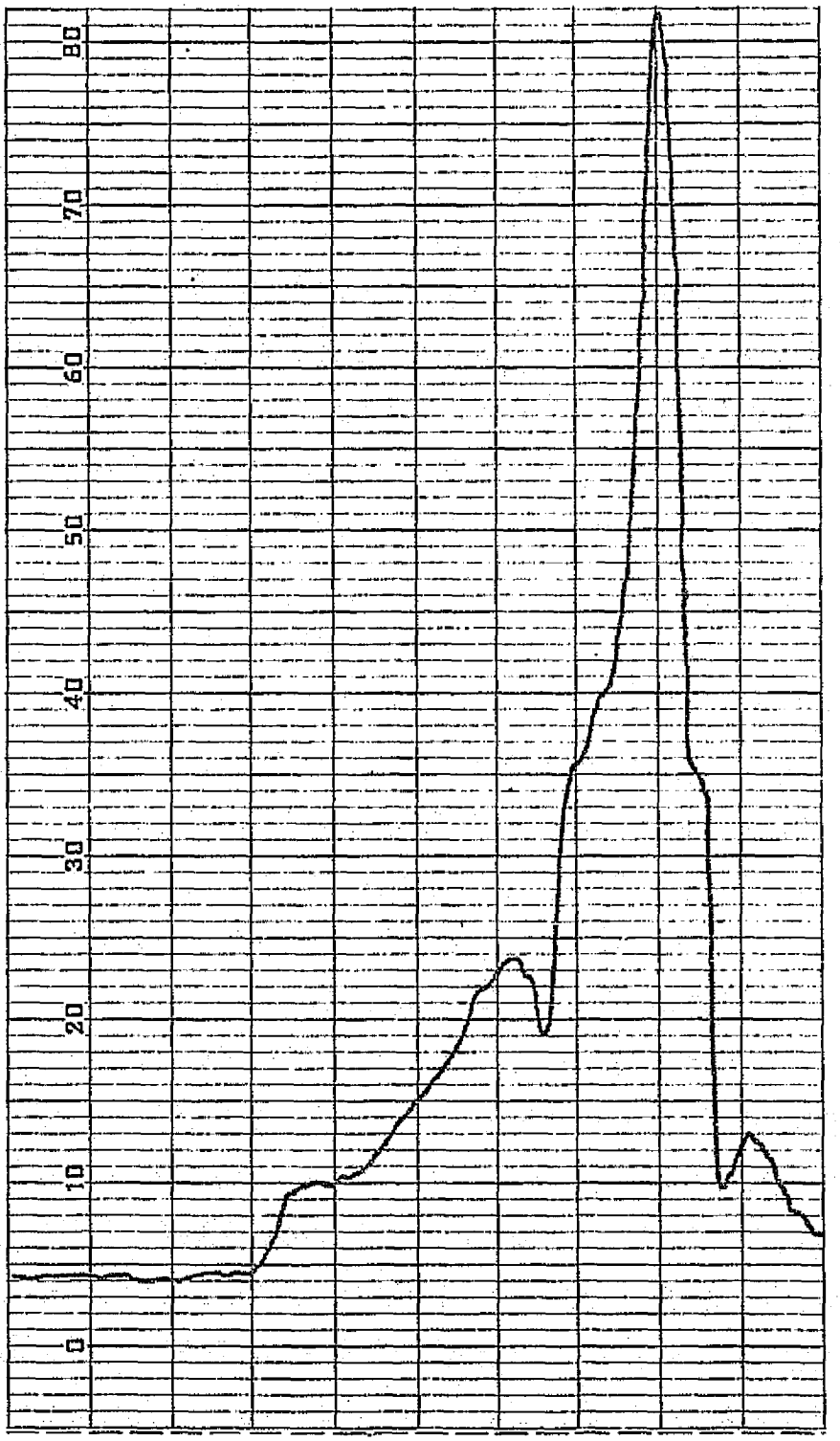

FIGURE 22. DENSITOMETER TRACE OF S-190B PHOTOGRAPH FOR TRANSECT THROUGH AVES ISLAND SHOWN IN FIGURE 21

Water depths can be extracted in this way from photographic transparencies, although with more difficulty and less reliability than from scanner data. The primary function of photography in this application is as an aid to the location of underwater features. However, water depths can be estimated from photography in the absence of scanner data, given the necessary controls on exposure, development and extrapolations.

4
CONCLUSIONS

The examples discussed in this report indicate that space acquired imagery can be an aid to the location of shallow water features and under certain conditions, bathymetry can be estimated. The S-190B photographs provide greater spatial resolution than either S-192 or LANDSAT MSS, but multispectral scanner data is more useful in distinguishing underwater features from surface phenomena and in providing estimates of water depth.

Significant improvement in depth penetration and spatial resolution over LANDSAT-1 data has been noted in Skylab scanner and photographic data. Skylab sensors have better band location, bandwidth, and gain characteristics than LANDSAT-1. However, the Skylab scanner has been plagued with noise and poor response characteristics, which have in some cases rendered the data less useful than LANDSAT-1 data. Attempts to use ratio depth processing have been less successful with Skylab than with LANDSAT data because of the noise in band 5. Methods of reducing noise by smoothing are less successful because of the conical scan configuration. However, the striping problem in LANDSAT due to differences in calibration of the six sensors is not present in Skylab.

The longer line length of Skylab data (1038 points as compared with 810 points in LANDSAT) and the larger number of data channels can cause some problems in data processing due to the limited storage capacity of some commonly available computer systems.

Coordination of data products and determination of orbital and sensor parameters has been more difficult with Skylab than with LANDSAT data. Despite these problems, however, Skylab has generated a large amount of useful data which could be exploited by the techniques reported here. They can contribute to the general store of hydro-

graphic information and solve specific problems where an up-to-date knowledge of shallow water bottom topography over a large area is needed.

5
RECOMMENDATIONS

Since the potential for remote bathymetry with the use of passive multispectral scanner from aircraft [1-3] and spacecraft has been demonstrated, further development and work should be aimed at improvements of the technique and in optimizing system parameters for best penetration and most accurate depth determinations. Skylab data supports the use of blue/green wavelengths for water penetration. The success of narrower band channels is also demonstrated in the improvement in water penetration of Skylab band 5 (0.50-0.55 μm) over that of band 4 of LANDSAT (0.5-0.6 μm).

Experience with low-altitude data [1-3] has indicated the optimum channels to be used with the ratio method for determining water depth as 0.55 - 0.58 μm and 0.58 - 0.63 μm. These wavelengths are probably not optimum for space platforms, because of the larger atmospheric effects and the lower signal-to-noise ratios obtainable with satellite systems. Nevertheless, the use of two or more bands for determining depths should be incorporated in future satellite systems because of the increased information available and also because of the increased potential for signal processing with two or more bands, e.g., ratio, subtraction, correlations, and averaging.

The use of to or more control points (where the depth is known) in a given scene for aiding in calculating water parameters such as water attenuation and bottom reflectance could be incorporated in future satellite operations. Either ship data taken in the day of an overpass or transmitting beacons from moored areas could provide the necessary ground control information. As a minimum, such information would consist of the water depth at the time of overpass. Additional measurements of the water attenuation and solar irradiance would also be useful.

Further theoretical formulations would be helpful on the effects of atmospheric attenuation, surface reflection, light scattering in water due to suspension, and changes in bottom reflectivity. These theoretical formulations would help in defining more precisely the optimum spectral intervals and band location for future MSS. Particular attention should be afforded to sensors with adequate signal to noise ratios and proper dynamic range of the transmitted signal for best measurements use.

APPENDIX

ERROR ANALYSIS

Three methods of extracting water depth from multispectral data have been mentioned in this report: the single-channel method, the ratio method, and the optimum-decision-boundary method. All three methods are subject to errors when the characteristics of the bottom, the water, transmission, or the surface reflection properties change. The magnitude of these errors are calculated for each of the three methods in this appendix. The ratio method yields the smallest error due to changes in the bottom and the water quality, but the largest error due to noise or changes in the surface-reflected signal. In addition, the ratio method requires the use of two channels which are relatively widely separated in wavelength, such as a green channel and a red channel [3]. Thus the maximum depth is limited by the penetration depth of the least penetrating channel. The optimum-decision-boundary technique has no such limitations on channel selection, and in fact gives the best results when two equally penetrating channels are used. The best method for any given application area then depends on the data quality, the channels available, and the type of changes occurring in the scene.

In this section, analytical expressions are given for the error (ΔZ) in the calculated depth due to changes in bottom reflectance ($\Delta\rho_b$) and water attenuation coefficient ($\Delta\alpha$), and to errors in the estimation of the bottom-reflected signal (ΔL_{bi}). The latter errors may be caused by system noise or by fluctuations in the surface-reflected radiance (L_s) or the atmospheric path radiance (L_p). These expressions are then evaluated for an arbitrary set of conditions and the total error is plotted versus depth for all three methods. This plot is not intended to indicate the actual error in any of the

situations described in this report, but is included only to illustrate the relative errors given by the three methods.

A.1 SINGLE CHANNEL METHOD

In our analysis, the total radiance observed over water is assumed to be the sum of three components.

$$L = L_p + L_s + L_b \tag{A-1}$$

where the first two components, L_p, the atmospheric path radiance, and L_s, the surface-reflected radiance, are assumed to be constant throughout the scene. The third component, L_b, the bottom-reflected radiance, has the following dependence on water depth Z:

$$L_b = L_o e^{-\alpha f Z} \tag{A-2}$$

where L_o = radiance at zero water depth,
α = water attenuation coefficient,
f = sec θ + sec ϕ,
θ = scan angle (under water)
ϕ = solar zenith angle (under water)

Inverting equation (A-2), the water depth using a single channel is given by:

$$Z = \frac{-1}{\alpha f} \ln\left(\frac{L_b}{L_o}\right) \tag{A-3}$$

The radiance at zero water depth, L_o, is directly proportional to the bottom reflectivity ρ_b. A change $\Delta\rho_b$ in the bottom reflectivity, therefore, leads to an error in the calculated depth of

$$\Delta Z_b = \frac{1}{\alpha f} \frac{1}{L_o} \left(\frac{\partial L_o}{\partial \rho_b} \right) \Delta \rho_b = \frac{1}{\alpha f} \left(\frac{\Delta \rho_b}{\rho_b} \right) \tag{A-4}$$

Likewise, a change in the attenuation coefficient α will yield an error

$$\Delta Z_\alpha = \frac{\Delta \alpha}{\alpha^2 f} \ln \left(\frac{L_b}{L_o} \right) = - \frac{\Delta \alpha}{\alpha} Z \tag{A-5}$$

If there is system noise or if there are fluctuations in the first two components of equation (A-1), the bottom-reflected signal L_b will be incorrectly measured. This error may be estimated by calculating the standard deviation of the radiances measured over deep water. For an error L_b the corresponding error in the calculated depth is

$$\Delta Z_n = \frac{1}{\alpha f} \frac{\Delta L_b}{L_b} = \frac{1}{\alpha f} \frac{\Delta L_b}{L_o} e^{\alpha f z} \tag{A-6}$$

Note that the error due to bottom changes is independent of depth, the error due to water attenuation changes is proportional to depth, and the error due to noise or surface fluctuations increases exponentially with depth. At large depths, therefore, the latter type of error is always predominant.

A.2 RATIO METHOD

In the ratio method, the radiance is measured in two channels, i and j, and the water depth is calculated using the following equation:

$$Z = \frac{1}{(\alpha_i - \alpha_j)f} \ln\left(\frac{L_{bi}}{L_{oi}} \frac{L_{oj}}{L_{bj}}\right) \tag{A-7}$$

If the bottom reflectivity in channel i changes by $\Delta\rho_{bi}$, and that in channel j changes by $\Delta\rho_{bj}$, the error in the calculated depth is

$$\Delta Z_b = \frac{1}{(\alpha_i - \alpha_j)f} \left(\frac{\Delta\rho_{bi}}{\rho_{bi}} - \frac{\Delta\rho_{bj}}{\rho_{bj}}\right) \tag{A-8}$$

The advantage of this method is that in some cases a pair of channels can be found in which the ratio of the bottom reflectivities remains constant throughout the scene, even though the reflectivities themselves may change. In such cases the error given by equation (A-8) reduces to zero.

The error due to changes in water attenuation is given by:

$$\Delta Z_\alpha = \frac{\Delta\alpha_i - \Delta\alpha_j}{\alpha_i - \alpha_j} Z \tag{A-9}$$

where $\Delta\alpha_i$ and $\Delta\alpha_j$ are the changes in the attenuation coefficient in channels i and j. If these changes are due to variations in concentration of a substance in suspension which does not exhibit significant spectral variation (e.g., sand), the changes in the attenuation coefficient are nearly the same for all wavelengths. In this case, the error from equation (A-9) again reduces to zero.

Finally, the error due to system noise or surface fluctuations is

$$\Delta Z_n = \frac{1}{(\alpha_i - \alpha_j)f} \left[\left(\frac{\Delta L_{bi}}{L_{oi}}\right)^2 e^{2\alpha_i fz} + \left(\frac{\Delta L_{bj}}{L_{oj}}\right)^2 e^{2\alpha_j fz}\right]^{1/2} \tag{A-10}$$

which is larger than the corresponding error using the single-channel method.

A.3 OPTIMUM DECISION BOUNDARY METHOD

In this method, the water depth is calculated as follows:

$$Z = \frac{1}{(\alpha_i^2+\alpha_j^2)f}\left[\alpha_i \ln\left(\frac{L_{bi}}{L_{oi}}\right) + \alpha_j \ln\left(\frac{L_{bj}}{L_{oj}}\right)\right] \qquad \text{(A-11)}$$

The error due to changes in bottom reflectivity is given by:

$$Z_b = \frac{1}{(\alpha_i^2+\alpha_j^2)f}\left(\alpha_i \frac{\Delta\rho_{bi}}{\rho_{bi}} + \alpha_j \frac{\Delta\rho_{bj}}{\rho_{bj}}\right) \qquad \text{(A-12)}$$

This error may be reduced by choosing two channels where the bottom reflectivities are negatively correlated. This is not possible for all bottom types, but may be possible for some types, such as green vegetation and sand.

The error due to changes in water attenuation is given by:

$$\Delta Z_\alpha = \frac{\alpha_i \Delta\alpha_i + \alpha_j \Delta\alpha_j}{\alpha_i^2 + \alpha_j^2} Z \qquad \text{(A-13)}$$

It is not possible to reduce this error to zero, because changes in the attenuation coefficient in two channels are always positively correlated. If the attenuation coefficient changes are the same in both channels, this error is intermediate between the corresponding errors using the single-channel method on each channel.

The error in this method due to noise or surface reflectance changes is

$$\Delta Z_n = \frac{1}{(\alpha_i^2 + \alpha_j^2) f} \left[\alpha_i^2 \left(\frac{\Delta L_{bi}}{L_{oi}} \right)^2 e^{2\alpha_i fz} + \alpha_j^2 \left(\frac{\Delta L_{bj}}{L_{oj}} \right)^2 e^{2\alpha_j fz} \right]^{1/2} \quad \text{(A-14)}$$

This error is smaller than that for the single-channel or ratio method if the two attenuation coefficients are equal or nearly equal.

A.4 TOTAL ERROR COMPARISON

These expressions were evaluated, and the total error calculated using the equation

$$(\Delta Z)^2 = (\Delta Z_b)^2 + (\Delta Z\alpha)^2 + (\Delta Z_n)^2 \quad \text{(A-15)}$$

for clear oceanic water at 0.55 μm (channel i) and 0.60 μm (channel j), with a 20 percent change in bottom reflectance and attenuation coefficient. A noise figure of 2 percent was used, which is less than the noise observed in our S-192 data, but is approximately equal to the noise we have seen in LANDSAT data (i.e., signals over deep water vary across 4 digital counts).

The smallest error at very shallow depths is obtained by the ratio method. However, the errors using this method increase very rapidly with depth. At large depths the least error is obtained using the single channel with the lowest attenuation coefficient. The optimum-decision-boundary method reduces the error when two channels with nearly equal attenuation coefficients are used. However, when the two channels are widely separated, as in this example, only a marginal improvement over the least penetrating channel is obtained.

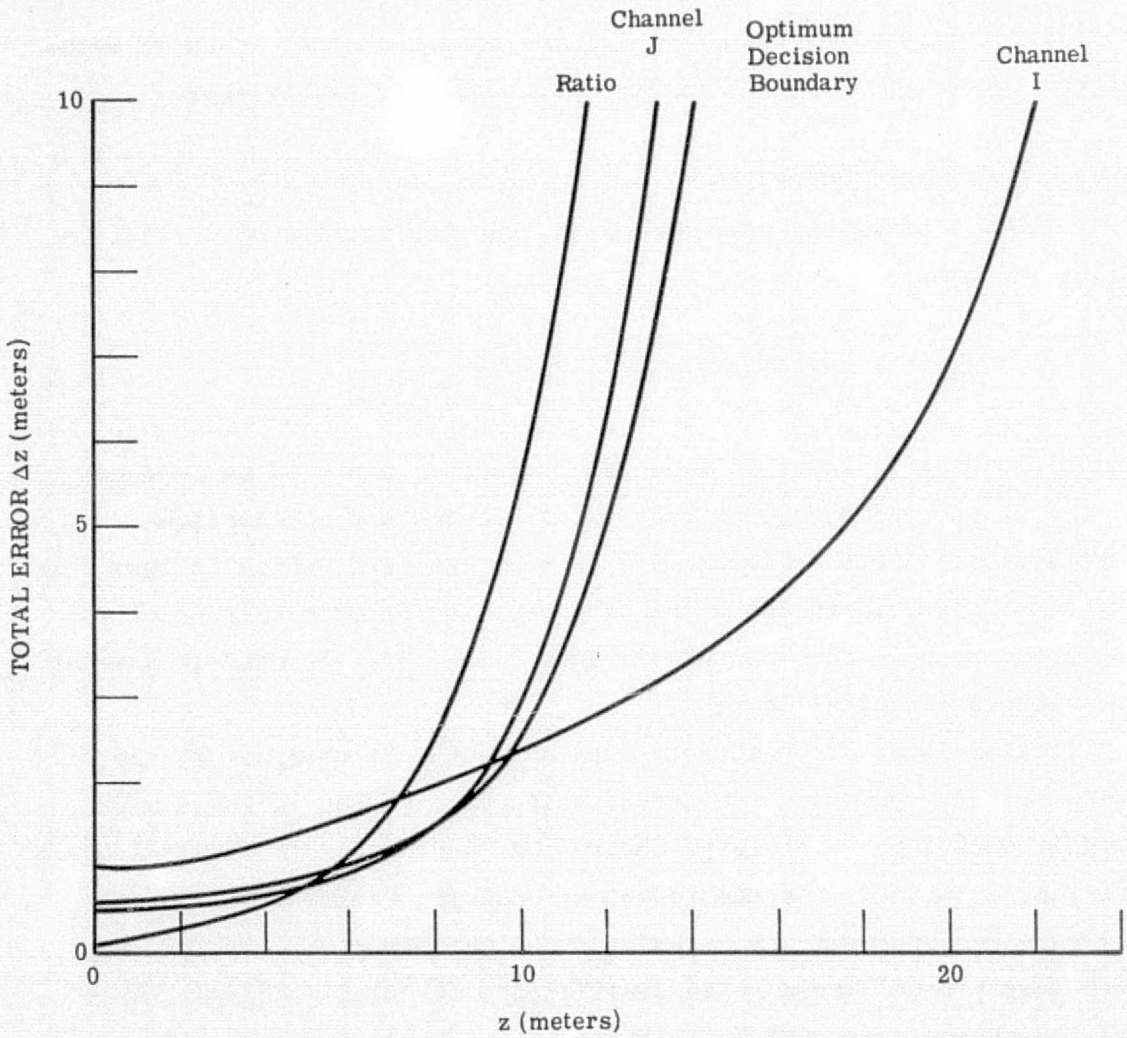

FIGURE 23. COMPARISON OF TOTAL ERROR FOR THREE DEPTH ALGORITHMS

REFERENCES

1. F.C. Polcyn and R.A. Rollin, "Remote Sensing Techniques for the Location and Measurement of Shallow-Water Features," Report No. 8973-10-P, Willow Run Laboratories, January 1969.

2. F.C. Polcyn, W.L. Brown, and I.J. Sattinger, "The Measurement of Water Depth by Remote Sensing Techniques," Report No. 8973-26-F, Willow Run Laboratories, October 1970.

3. W.L. Brown, F.C. Polcyn, A.N. Sellman, and S.R. Stewart, "Water Depth Measurement by Wave Refraction and Multispectral Techniques," Report No. 31650-31-T, Willow Run Laboratories, August 1971.

4. F.C. Polcyn and D.R. Lyzenga, "Remote Bathymetry and Shoal Detection with ERTS", Report No. 193300-51-F, Environmental Research Institute of Michigan, April 1975.

5. J.V.A. Trumbull, personal communication, April 11, 1975.

6. P.G. Hasell, Jr., et al., "Michigan Experimental Multispectral Mapping System - A Description of the M-7 Airborne Sensors and its Performance", Report No. 190900-10-T, Environmental Research Institute of Michigan, January 1974.